Journal of Holography Applications in Physics
Volume 6, Issue 4, Summer 2026, 185–216
©Available online at http://jhap.du.ac.ir
DOI: 10.22128/jhap.2026.3248.1191
Online ISSN: 2783–3518

Regular article

Testing Logarithmic $f(G)$ Model with Observational Data Sets

Mohit Thakre[1] · Praveen Kumar Dhankar[2] · Albert Munyeshyaka[3] · Safiqul Islam[4]

[1] Symbiosis Institute of Technology, Nagpur Campus, Symbiosis International, Deemed University, Pune-440008, Maharashtra, India;
Email: mohitthakre100@gmail.com

[2] Symbiosis Institute of Technology, Nagpur Campus, Symbiosis International, Deemed University, Pune-440008, Maharashtra, India;
E-mail: pkumar6743@gmail.com

[3] Rwanda Astrophysics Space and Climate Science Research Group, University of Rwanda, College of Science and Technology, Kigali, Rwanda;
Corresponding Author E-mail: munalph@gmail.com

[4] Department of Mathematics and Statistics, College of Science, King Faisal University, P.O. Box 400, Al Ahsa 31982, Saudi Arabia.
E-mail: sislam@kfu.edu.sa

Received: February 9, 2026; **Accepted:** April 9, 2026

Abstract. In this study, we have put the mechanism for a Friedmann equation of modified f(G) gravity by solving it with numerical method in the view of matter with pressure-less condition. This mechanism allows us to forecast the redshift action of expansion rate of the Hubble. Here, in this paper, we have applied a Bayesian Markov Chain Monte Carlo (MCMC) technique, which is applying late time cosmic observances to put limitation on the model parameters of the Gauss Bonnet. Our understanding results in the fact that the $f(G)$ model can restore low redshift action of the standard (Λ CDM) model. We have used Hubble (OHD), Pantheon and RSD for MCMC analysis of the logarithmic model of $f(G)$ and to constrain parameters including Ω_m and H_0.

Keywords: Cosmic Acceleration; Gravity; Observational Data; MCMC Analysis.

Contents

1 Introduction

Einstein developed general relativity (GR) in 1915 as a result of his works to recognize the gravitational pull. Describing gravity as the space-time curvature produced about by the presence of energy and mass [1]. Dark matter [2], dark energy (DE; [3]) and the accelerated expansion of the Universe [4] are between the phenomena that GR finds difficult to fully illustrate, in spite of having passed many experiments [5] and continuing to be the foundation of concurrent gravitational physics. Several impotent premises of gravity have been proposed in reaction to these tribulations [6].

The latest observational data, such as the Dark Energy Spectroscopic Instrument (DESI) examinations [7], Type Ia supernovae (SNe Ia; [4,8]), the Wilkinson Microwave Anisotropy Probe experiment (WMAP; [9]), the cosmic microwave background (CMB; [10], the Baryon Oscillation Spectroscopic Survey (BOSS; [11], and the baryon acoustic oscillations (BAO) data sets [12], have guided researchers to evolve and modify the elementary notions of General Relativity. The new observational documentation is considered to be better accommodated and resolute by these optional ideas.

The $f(R)$ is a gravity for which f denotes the arbitrary function of Ricci scalar R, known as modest evolution of Einstein's gravity [13]. For the metric tensor, the equations of motion do not contain derivative terms larger than two according to these theories. The Gauss Bonnet (GB) term only aids to the equations of motion when linked with form like $f(\phi G)$ containing scalar field ϕ [14], since denotes $\sqrt{-g}\,G$ total derivative . This kind of compile produced in the string theory's low energy efficient action by a dilaton graviton mixing term [15]. Constructing feasible $f(R)$ models that satisfy local gravity and cosmic constraints is difficult, clearly in this comparatively basic situation. This complexity results from a strong relation among $f(R)$ gravity which introduced non-relativistic matter and Dark Energy (DE) in the Einstein frame [16–26]. $f(G)$ gravity is one such premise that has attracted a lot of attention. G which is a GB invariant give linear combination of terms containing Ricci scalar R, the Ricci tensor R_{ij}, and the Riemann tensor R_{ijkl} [17,27–30], this theory changes the Einstein Hilbert action. Together with R, it is a member of the Lovelock scalars, an infinite class of curvature invariants.

The potentiality of $f(G)$ gravity to demonstrate the followed late-time cosmic acceleration in the Universe is what makes it interesting. Instead of an uncommon source of matter with negative pressure, this acceleration might be due to a change in gravity [31]. To comprehend the nature of dark energy (DE), an excellent deal of study has been done newly on modified gravity [32]. Because modified gravity models are more in line with local gravity tests and cosmic observations than models rested on exotic matter sources, they are particularly fascinating [33]. The Shift from deceleration to acceleration and the current accelerated expansion of the Universe which are most interesting elements of late time cosmology [17,20,34,35], may be explained by this theory, which is notion to be able to pass Solar System experiments [20,35].

One of the most demanding challenges in any modified theory of gravity is to reach to a viable and physically consistent functional form of the gravity model. While certain theoretical huddles such as the presence of Noether symmetries, the presence of Ghost and the stability of perturbations can be analysed at theoretical level, these considerations alone are not sufficient. It is advised that the proposed theory should be tested against different observational data to assess its physical relevance and validity[36]. In this regard, many observational works on solar system data [37] and on cosmological data [38–40], such as the confrontation with supernovae type Ia data, cosmic microwave background (CMB), baryonic acoustic oscillations (BAO) and Hubble data have been tried [36]. Some of the impressive

works in this context have been published. One can mention the work presented in [41], where the authors constrained cosmological physics by employing three sets of non-Planck CMB data and obtained a more stringent constraint on the Hubble constant compared to non-DESI-BAO data+non-Planck CMB data, as well as reducing the significance of the Hubble tension. The work presented in [42] reevaluated the tension H_0 with the joint analysis of non-Planck CMB and DESI BAO and and the results found are in agreement with the one published in [41]. The work presented in [43], discussed cosmological constraints on dark-energy models using DESI BAO measurements, proving that combining these newly late universe probes can significantly improve constraints on cosmological parameters. It was argued that the present combination can effectively break parameter degeneracies.

A number of researchers have explored modified Gauss-Bonnet gravity, written as $f(G)$, as a compelling extension of general relativity capable of accounting for different phase of cosmic evolution. In Ref. [44], an $f(G)$ model was reconstructed base on an exponential scale factor demonstrating the realisation of a bouncing cosmology. Their asymptotic analysis further indicated compatibility with late-time cosmic acceleration. In a related study [45], cosmological perturbations within the framework of $f(G)$ gravity coupled to a scalar field were analysed using the $1+3$ covariant approach. The results showed that the evolution of matter over-densities fluctuations differs markedly from the predictions of the standard ΛCDM model, primarily due to additional effects introduced by the scalar field. Meanwhile, Ref. [46] addressed the theoretical consistency of $f(G)$ gravity, demonstrating that such models can satisfy solar system constraints, while naturally describing the transition from a decelerated to an accelerated expansion phase. In addition, [47] focused on reconstructing observationally viable $f(G)$ models, highlighting their agreement with cosmological dynamics inferred from data. Collectively, these studies underscore the potential of $f(G)$ gravity to provide a comprehensive description of both the background expansion and the perturbative structure formation of the universe beyond the framework of general relativity.

Motivated by the aforementioned studies, we intend to place constraints on the parameters of a modified Gauss-Bonnet gravity framework. For illustrative and pedagogical purposes, we focus on a logarithmic form of the $f(G)$ gravity model. After deriving the corresponding modified Friedmann equation, our aim is to constrain the parameters of the considered $f(G)$ model through a Bayesian analysis using Hubble parameter measurements, the Pantheon Plus and redshift space distortion (RSD) observations. To this end, we numerically solve the modified Friedmann equation under the assumption that the universe is dominated by pressure-less dust matter, characterized by a vanishing equation of state parameter. Vibrant cosmological observations, such as Observational Hubble Data (OHD), DESI BAO, Pantheon Type Ia Supernovae (SNeIa) and RSD, have been applied by using the Markov Chain Monte Carlo (MCMC) method to constrain models of modified gravity [59–67]. Subsequently, we employ Markov Chain Monte Carlo (MCMC) techniques to estimate the model parameters within the $f(G)$ context. As part of the analysis, we generate corner (triangular) plots and report the mean values of the parameters constrained by individual datasets, namely i) Hubble parameter measurements, ii) Pantheon Plus and iii) RSD data. Furthermore, we extend our investigation by performing joint analysis using different combinations of the aforementioned datasets.

Finally, we conduct a statistical model comparison to assess the performance of the proposed $f(G)$ gravity model relative to the standard ΛCDM cosmology. In this regard, we employ the Akaike Information Criterion (AIC), Deviance Information Criterion (DIC) and the Bayesian Information Criterion (BIC), which provide quantitative measures of the model's statistical viability. For completeness of the work, we provide a qualitative discussion on the energy conditions of the proposed model. Furthermore, the stability of the model will be examined through dynamical systems and the associated phase space.

The rest of this paper is organized as follows: In Section 2, we present the mathematical framework, where the cosmological equations are discussed in the context of $f(G)$ gravity. In Section 3, we describe the data and methodology employed to constrain the $f(G)$ model parameters. This section also discusses the results. Sections 4 and 5 present energy conditions and stability analysis, respectively whereas Section 6 is reserved for the conclusions.

2 Mathematical framework and Background equations in the Context of $f(G)$ gravity

In the present section, we modify the Einstein-Hilbert action for GR and discuss the field equations in the context of $f(G)$ gravity. We then present the formulation of logarithmic function of $f(G)$ to be used in constraining model parameters.

2.1 Hilbert action on $f(G)$

Einstein Hilbert action on $f(G)$ function is given by

$$S = \int \sqrt{-g}\left[\frac{R}{2\kappa^2} + \mathcal{L}_m + f(G)\right] d^4x, \tag{2.1}$$

where $\kappa^2 = G_N 8\pi = 1$, G_N is the constant of Newtonian and $\mathcal{L}_m$ denotes the matter Lagrangian. The Gauss Bonnet term is defined as

$$G = R^2 - 4R_{ij}R^{ij} + R_{ijkl}R^{ijkl}. \tag{2.2}$$

Varying the action over g_{ij} [48], we get the following equation:

$$\begin{aligned} 0 = {} & \frac{1}{2\kappa^2}\left(-R^{ij} + \frac{1}{2}g^{ij}R\right) + T^{ij} + \frac{1}{2}g^{ij}f(G) - 2f_G R R^{ij} \\ & + 4f_G R^i_r R^{jr} - 2f_G R^{irl\tau}R^j_{rl\tau} - 4f_G R^{ir\nu l}R_{rl} \\ & + 2\left(\nabla^i\nabla^j f_G\right)R - 2g^{ij}(\nabla^2 f_G)R - 4(\nabla^r\nabla^i f_G)R^j_r \\ & - 4(\nabla^r\nabla^j f_G)R^i_r + 4(\nabla^2 f_G)R^{ij} + 4g^{ij}(\nabla_r\nabla_l f_G)R^{rl} \\ & - 4(\nabla_r\nabla_l f_G)R^{irjl}. \end{aligned} \tag{2.3}$$

where consider the notations $f_G = \frac{df}{dG}$ and $f_{GG} = \frac{d^2 f}{dG^2}$.

Metric for spatially flat FLRW universe is

$$ds^2 = -dt^2 + a(t)^2[(dx^1)^2 + (dx^2)^2 + (dx^3)^2], \tag{2.4}$$

where $a(t)$ is the scale factor at cosmological time t.

Ricci scalar R and Gauss Bonnet term G can be defined as functions of the Hubble parameter as following:

$$R = 6\left(\dot{H} + 2H^2\right), G = 24\left(\dot{H}H^2 + H^4\right), \tag{2.5}$$

Metric (2.4) has the field equations, gives the FLRW equations in the form:

$$3H^2 = \kappa^2(\rho_{\rm m} + \rho_{\rm r} + \rho_{\rm DE}) = \kappa^2\rho_{\rm eff}. \tag{2.6}$$

$$(2\dot{H} + 3H^2) = -\kappa^2 \left(\frac{\rho_r}{3} + p_{\rm DE}\right) = -\kappa^2 p_{\rm eff},, \tag{2.7}$$

where H denotes the Hubble parameter, ρ_m shows matter density, ρ_r shows the radiation density and $\rho_{\rm DE}$ shows the Dark energy density. Also, dot signifies a derivative with respect to cosmic time t. Moreover, the effective Dark Energy (DE) density and pressure is given as follows:

$$\rho_{\rm DE} = \frac{1}{\kappa^2}\left[Gf_G - f(G) - 24\dot{G}H^3 f_{GG}\right], \tag{2.8}$$

$$p_{\rm DE} = \frac{1}{\kappa^2}\left[8H^2\ddot{f}_G + 16H(\dot{H} + H^2)\dot{f}_G + f - Gf_G\right]. \tag{2.9}$$

Distinctly these factors ensue their respective conservation laws $\dot{\rho}_m + 3H\rho_m = 0$ and $\dot{\rho}_r + 4H\rho_r = 0$. From Equations (2.6) and (2.7), the DE density and pressure standard evolution equation can be written as follows:

$$\dot{\rho}_{\rm DE} + 3H\left(\rho_{\rm DE} + p_{\rm DE}\right) = 0. \tag{2.10}$$

Effective DE EoS parameter is defined as follows:

$$\omega_{\rm DE} = \frac{p_{\rm DE}}{\rho_{\rm DE}}. \tag{2.11}$$

For the ΛCDM limit, the EoS parameter $\omega_{DE} \implies -1$.

2.2 Formulisation of logarithmic function of $f(G)$

Given the numerous cosmic data analysis and experiments carried out within our solar system, all of which support the tenets of general relativity. It can be inferred that any deviations from conventional GR should be minimal. The logarithmic function of $f(G)$ is given by

$$f(G) = \frac{\sqrt{3G}}{2}\, ln(\gamma G). \tag{2.12}$$

Consider the matter acts like a perfect fluid under the condition of pressure. The matter density is defined as $\rho_m = 3H_0^2\Omega_{m0}(1+z)^3$, where z is the cosmological redshift which is defined as $\frac{a_0}{a} = 1 + z$ and a_0 shows the scale factor at current and a indicates the scale factor when the light emitted and Ω_{m0} is the matter density parameter's current value.

As we know that

$$\dot{H} = \frac{dH}{dt} = H'(z)[-(1+z)H],$$

$$\dot{H} = -(1+z)HH'.$$

From Equation (2.5), we can write

$$\dot{G} = -24(1+z)H^3[3H'S - (1+z)HH''],$$

where,

$$S = H - H'(1+z).$$

Now we compute the values of $f_G \quad and \quad f_{GG}$. So by using Equation (2.5), we get

$$f_G = \frac{\sqrt{3}}{2\sqrt{G}}\left[1 + \frac{1}{2}\, ln(\gamma G)\right], \tag{2.13}$$

$$f_{GG} = -\frac{\sqrt{3}}{8G^{3/2}}\ ln(\gamma G). \tag{2.14}$$

From Equation (2.8), (2.13) and (2.14), and using value of ρ_m, Equation (2.6) becomes

$$\begin{aligned} 3H^2 = &-\frac{12\sqrt{3}H^2}{\sqrt{G}}\Big((1+z)HH' - H^2\Big)\Big[1+\frac{1}{2}ln(\gamma G)\Big] \\ &-\frac{\sqrt{3G}}{2}\ ln(\gamma G) - \frac{72\sqrt{3}}{G^{3/2}}H^6(1+z)\Big[3H'S - (1+z)HH''\Big] \\ &+3H_0^2\Omega_{m0}(1+z)^3. \end{aligned} \tag{2.15}$$

This is the second order differential equation for the function $H(z)$ which can be solved using boundary condition in which first initial condition is $H(0) = H_0$. For getting second initial condition, at present, as the first derivative of Hubble parameter is coherent with observational prophecies of Λ CDM model, which is given by following expansion law:

$$H_{\Lambda CDM} = H_0\sqrt{1-\Omega_{m0}+\Omega_{m0}(1+z)^3}. \tag{2.16}$$

We gets the second initial condition for Equation (2.15) by differentiating Equation (2.16) with respect to z and which results into the $H'(0) = \frac{3}{2}H_0\Omega_{m0}$.

3 Data analysis and Discussion of the Results

In this section, we have placed observational constraints on the $f(G)$ gravity model which referred to Model I. Also, comprehensive statistical investigation is performed by comparing theoretical predictions of the $f(G)$ gravity models in association with cosmological observations. Particularly, parameters (Ω_m, γ, h) of the model are constrained by using cosmological observations through the Markov Chain Monte Carlo mechanism [49].It have to be noted that the parameter h is associated to the current Hubble rate by $h = H_0/100\,\mathrm{km\,s^{-1}\,Mpc^{-1}}$. The observational data sets such as Pantheon Plus [50], Hubble parameter measurements [51] and redshift space distortion (RSD) data have employed to constrain the model of $f(G)$ gravity. For the observational dataset, we have considered combinations as:

- **Dataset I**: PP+CC.
- **Dataset II**: PP+RSD.
- **Dataset III**: CC+RSD.

3.1 Statistical analysis

In the current years, cosmological models have been put out using different types of observational dataset. To compare these models with cosmological observations is the only route to see which are promoted by documentation. To get with suitable manner, we need to use comprehensive statistical method. Usually cosmology depends on Bayesian methods, estimation of parameter is generally done by using Bayesian diagnosis. In this case, the chi-square function (χ^2) and the likelihood function $(\mathcal{L})$ are connected according to the relation

$$\chi^2(\theta) = -2\ln\mathcal{L}(\theta). \tag{3.1}$$

Also we have used both the corrected Akaike Information Criterion (AIC_c) [52] and the Bayesian Information Criterion (BIC) [53], which are defined below as:

$$\mathrm{AIC}_c = \chi^2_{\min} + 2\mathcal{K}_f + \frac{2\mathcal{K}_f(\mathcal{K}_f+1)}{\mathcal{N}_t - \mathcal{K}_f - 1}, \tag{3.2}$$

and

$$\mathrm{BIC} = \chi^2_{\min} + \mathcal{K}_f \ln(\mathcal{N}_t), \tag{3.3}$$

Where, $\chi^2_{\min}$ denotes the minimum chi-square value, $\mathcal{N}_t$ is the total number of data points and $\mathcal{K}_f$ represents the number of free parameters. The model which has lowest AIC_c and BIC values is recognized by the data and is selected as the reference model. We have also introduced more influential selection criterion called Deviance Information Criterion (DIC) is defined as [54]-[55]

$$DIC = D(\bar{\theta}) + 2P_D, \tag{3.4}$$

where $P_D = D\bar{(\theta)} - D(\bar{\theta})$ and $D(\bar{\theta}) = \xi^2_{min}(\bar{\theta}) + K$, where θ is the vector parameters, K is a constant depending on the data and $D(\theta)$ is the deviance of the likelihood. The over-bars denote the average taken over the posterior distribution. To quantify the performance of other models relative to the reference, we compute the differences:

$$\Delta\mathrm{AIC}_c = \mathrm{AIC}_{c,\mathrm{model}} - \mathrm{AIC}_{c,\Lambda\mathrm{CDM}}, \tag{3.5}$$

$$\Delta\mathrm{BIC} = \mathrm{BIC}_{\mathrm{model}} - \mathrm{BIC}_{\Lambda\mathrm{CDM}}, \tag{3.6}$$

$$\Delta\mathrm{DIC} = \mathrm{DIC}_{\mathrm{model}} - \mathrm{DIC}_{\Lambda\mathrm{CDM}} \tag{3.7}$$

The interpretation of $\Delta\mathrm{AIC}_c$ (and analogously ΔBIC and ΔDIC) is as follows: $\Delta IC \leq 2$[1] indicates substantial observational support for the fitted data, $2 < \Delta IC \leq 6$ indicates moderate support, $6 < \Delta IC \leq 10$ indicates weak support, and $\Delta IC > 10$ signifies no observational support.

3.2 Hubble data

To estimate the Hubble parameter $H(z)$ [56,57], we have use differential age (cosmic chronometer) mechanism. We have used 30 observational data points of $H(z)$ which has a range of redshift $0.07 < z < 1.965$. The χ^2 formula is given by

$$\chi^2_H = \sum_{i=1}^{30} \frac{(H_{\mathrm{th}} - H_{\mathrm{obs}})^2}{\sigma_i^2}, \tag{3.8}$$

where $\sigma_{H(z_i)}$ represents standard error, H_{th} represents the theoretical prediction of the Hubble parameter and H_{obs} represents the observed value of the Hubble parameter which we have taken into account.

The combined allocations of the model parameter Ω_{m0}, H_0, and γ developed using a MCMC inspection using (OHD) dataset are shown by the corner plot in Figure 1. The one-dimensional marginalization probability allocations for each parameter are shown in diagonal panels simultaneously, with their 68% confidence intervals. The two-dimensional relationship contours between couples of parameters are described in off diagonal panels; The plot denotes two confidence levels contours analogous to 1σ confidence level and 2σ confidence level, where the inner blue area shows the 1σ uncertainty and outer light blue shaded region shows 2σ uncertainty. Due to Gaussian distributions, the parameters are

[1] N.B. ΔIC represents both ΔAIC and ΔBIC.

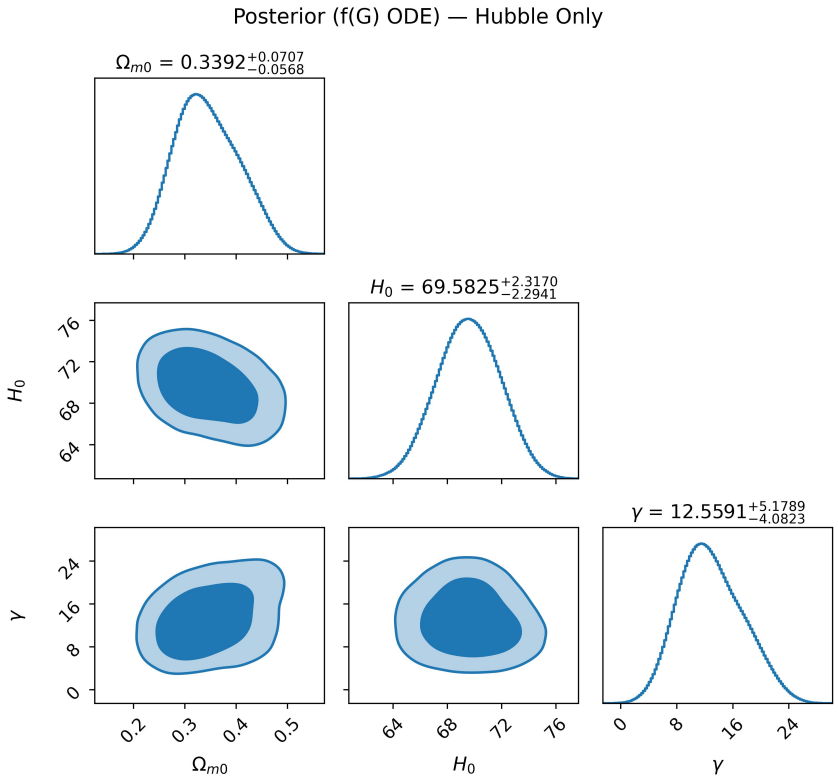

Figure 1: Confidence contours and marginalized posterior distributions for the parameters Ω_{m0}, H_0, and γ obtained from the Hubble (OHD) dataset.

highlight to be fine limitation, indicating true convergence and accurately evaluated. The model selection statistics shows that $\mathrm{AIC}_{\mathrm{model}} = 18.5165$ and $\mathrm{BIC}_{\mathrm{model}} = 22.7201$ and $\mathrm{DIC}_{\mathrm{model}} = 14.7835$ with $\Delta\mathrm{AIC}_{\mathrm{model}} = 2.4740$ and $\Delta\mathrm{BIC}_{\mathrm{model}} = 3.8752$ and $\Delta\mathrm{DIC}_{\mathrm{model}} = 2.7410$. An awesome consent between the model and the observational data is implicit by the reduced chi-square $\chi^2_{\mathrm{red}} = 0.4636$, which has the associated chi-square value at the MAP point, $\chi^2 = 12.5165$. Applying observational $H(z)$ data and associated error bases, Figure 2 compares the conventional Λ CDM cosmology with the rebuilt Hubble parameter $H(z)$ from the maximum a posteriori (MAP) model. The black dash curve shows the Λ CDM fit. The blue curve denotes the best fit prophecy of the MAP model, while the white dots indicate the observed Hubble parameter values at different redshifts. The MAP model indicates a barely larger expansion rate at higher redshifts, but it nearly matches the observational data and remains coherent with the Λ CDM. This consistency inside observational errors rises the indicated model's symmetry with current cosmological observations by showing that it works for a reliable and precise account of the cosmic expansion history.

3.3 RSD dataset

In the view of general relativity actions, the growth rate of cosmological perturbations is well defined by a following parametrization,

$$f(a) = \Omega_m(a)^{\beta(a)},$$

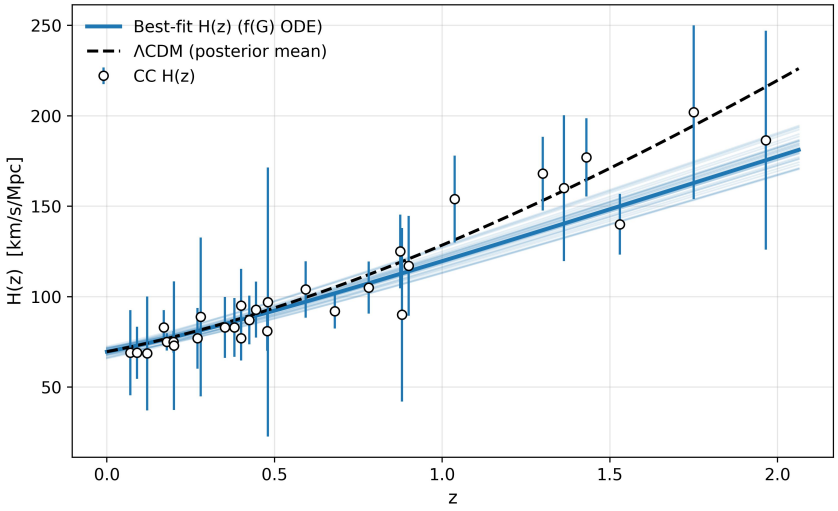

Figure 2: Comparison of the reconstructed Hubble function H(z)(blue curve) with observational H(z) data (blue lines with circular dots) and the ΛCDM prediction (black dashed curve).

$$\Omega_m(a) \equiv \frac{\Omega_{0m}}{a^3 H(a)^2/H_0^2},$$

$$\beta(a) = \frac{\ln f(a)}{\ln \Omega_m(a)}.$$

Here, we have considered ΛCDM cosmology.

Take a parametrization of the form [58]

$$f\sigma_8(z) = \lambda\,\sigma_8\,\frac{[\Omega_m(z)]^\beta}{(1+z)^\alpha},$$

where,

$$\Omega_m(z) = \frac{\Omega_{0m}(z+1)^3}{\Omega_{0m}(z+1)^3 + 1 - \Omega_{0m}}$$

χ^2 function for RSD is

$$\chi^2_{\rm RSD} = \sum_{i=1}^{N} \frac{\left[f\sigma_8^{\rm obs}(z_i) - f\sigma_8^{\rm th}(z_i)\right]^2}{\sigma_i^2}.$$

The combined allocations of the model parameter Ω_{m0}, H_0, γ and σ_8 developed using a MCMC inspection using (RSD) dataset are shown by the corner plot in Figure 3. The one-dimensional marginalization probability allocations for each parameter are shown in diagonal panels simultaneously, with their 68% confidence intervals. The two-dimensional relationship contours between couples of parameters are described in off diagonal panels; The plot denotes two confidence levels contours analogous to 1σ confidence level and 2σ confidence level, where the inner blue area shows the 1σ uncertainty and outer light blue shaded region shows 2σ uncertainty. Due to Gaussian distributions, the parameters are highlight to be fine limitation, indicating true convergence and accurately evaluated. The model selection statistics shows that $\mathrm{AIC_{model}} = 54.7288$ and $\mathrm{BIC_{model}} = 63.3014$ and $\mathrm{DIC_{model}} = 48.9108$

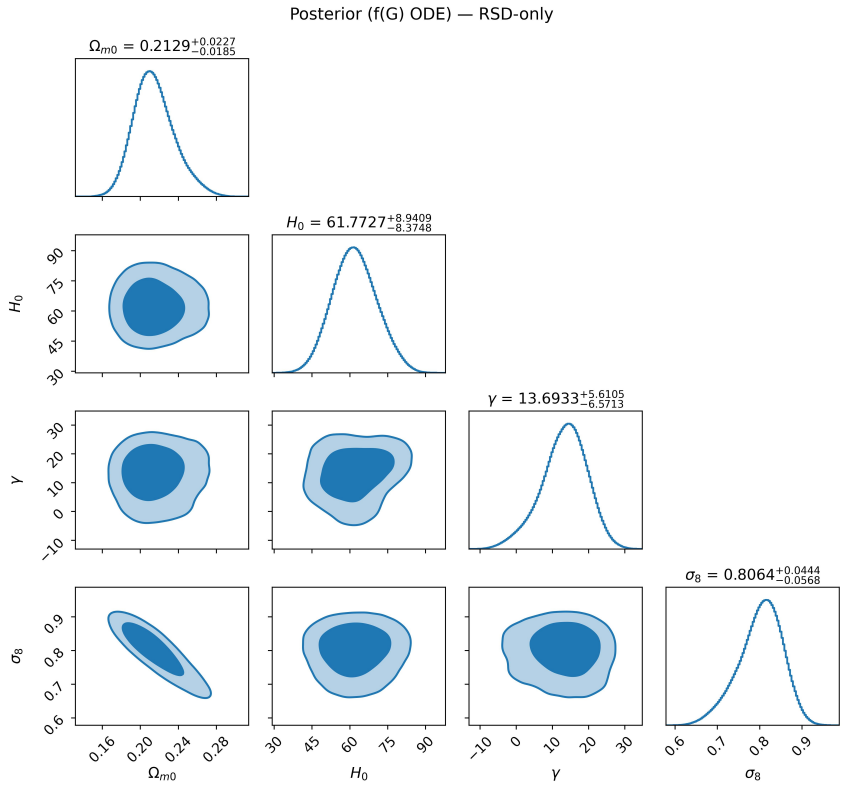

Figure 3: Confidence contours and marginalized posterior distributions for the parameters Ω_{m0}, H_0, γ and σ_8 obtained from the Hubble (RSD) dataset.

with $\Delta\text{AIC}_{\text{model}} = 5.3474$ and $\Delta\text{BIC}_{\text{model}} = 9.6337$ and $\Delta\text{DIC}_{\text{model}} = 3.5294$. An awesome consent between the model and the observational data is implicit by the reduced chi-square $\chi^2_{\text{red}} = 0.7920$, which has the associated chi-square value at the MAP point, $\chi^2 = 46.7288$.

The figure 4 relates the sigma function $f\sigma_8(z)$ (blue curve) with observational RSD data (blue lines with circular dots). For visual analogy, the average Λ CDM model is illustrated by the black dashed curve. Above the whole redshift range ($0.0010 \leq z \leq 1.9440$), the rebuilt model and the observational data overlap nearly, indicating a good match and high degree of consistency with observational measurements, showing that the indicated model successfully emulates the observed cosmic acceleration while keeping compliance with the mainstream cosmological framework.

3.4 Pantheon dataset

Distance moduli for the Pantheon dataset is shown as follows:

$$\mu = m - M_B = 5\log_{10}(D_L) + \mu_0,$$

where M shows the absolute magnitude and m shows the apparent magnitude and the nuisance parameter is given as $\mu_0 = 5\log\left(H_0^{-1}/\text{Mpc}\right) + 25$ [59].

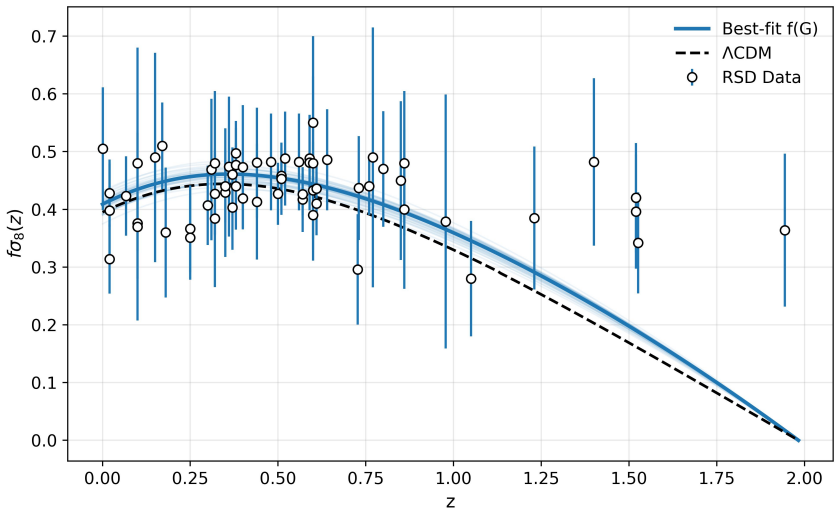

Figure 4: Comparison of the reconstructed sigma function $f\sigma_8(z)$ (blue curve) with observational RSD data (blue lines with circular dots) and the ΛCDM prediction (black dashed curve).

The luminosity distance ($D_L(z)$) is defined as

$$D_L(z) = \frac{c(1+z)}{H_0} \int_0^z \frac{dz^*}{E(z^*)},$$

For the Pantheon (SNIa) datasets, the χ^2 function is given by

$$\chi^2_{SN}(\phi^{\nu}_s) = \mu_s C^{-1}_{s,\mathrm{cov}} \mu^T_s .$$

The combined allocations of the model parameter Ω_{m0}, H_0, and γ developed using a MCMC inspection using (Pantheon) datasets are shown by the corner plot in Figure 5. The one-dimensional marginalization probability allocations for each parameter are shown in diagonal panels simultaneously, with their 68% confidence intervals. The two-dimensional relationship contours between couples of parameters are described in off diagonal panels; The plot denotes two confidence levels contours analogous to 1σ confidence level and 2σ confidence level, where the inner blue area shows the 1σ uncertainty and outer light blue shaded region shows 2σ uncertainty. Due to Gaussian distributions, the parameters are highlight to be fine limitation, indicating true convergence and accurately evaluated. The model selection statistics shows that $\mathrm{AIC}_{\mathrm{model}} = 866.9189$ and $\mathrm{BIC}_{\mathrm{model}} = 881.7800$ and $\mathrm{DIC}_{\mathrm{model}} = 862.5687$ with $\Delta\mathrm{AIC}_{\mathrm{model}} = 4.8475$ and $\Delta\mathrm{BIC}_{\mathrm{model}} = 9.8011$ and $\Delta\mathrm{DIC}_{\mathrm{model}} = 4.4972$. An awesome consent among the model and the observational dataset is inferred by the reduced chi-square $\chi^2_{\mathrm{red}} = 0.8246$, which has the associated chi-square value at the MAP point, $\chi^2 = 860.9189$.

The figure 6 compares the observational data and Pantheon Type la Supernovae (blue points with error bars) with the theoretical distance modulus $\mu(z)$ read by the rebuilt cosmological model (Solid red line). For sighted analogy, the average Λ CDM model is illustrated by the black dashed curve. Above the whole redshift range which is $0 < z < 2.5$, the rebuilt model and the observational data overlap nearly, indicating a good match and high degree of consistency with observational measurements, showing that the indicated

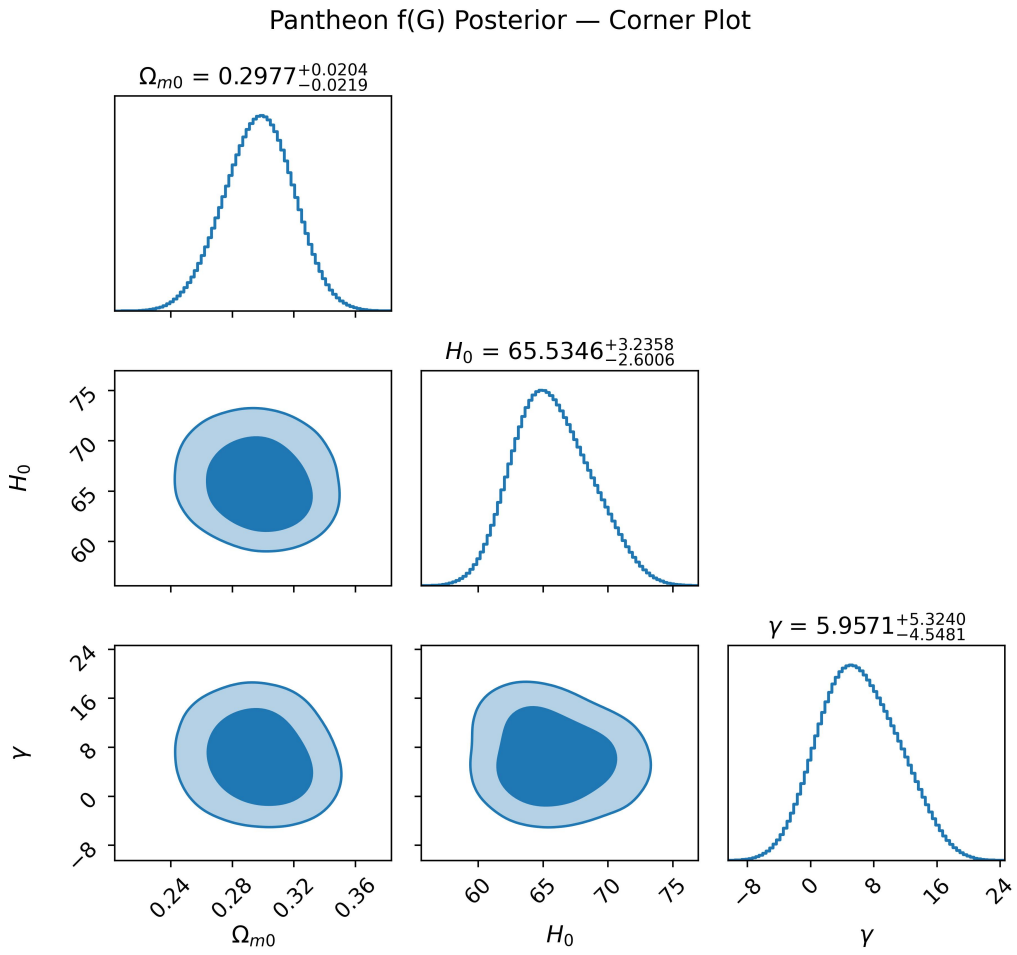

Figure 5: Confidence contours and marginalized posterior distributions for the parameters Ω_{m0}, H_0 and γ obtained from the (Pantheon) dataset.

model successfully emulates the observed cosmic acceleration while keeping compliance with the mainstream cosmological framework.

3.5 Mix datasets

The combined allocations of the model parameter Ω_{m0}, H_0, $\sigma_8$and γ developed using a MCMC inspection obtained from the (Hubble+RSD) dataset. are shown by the corner plot in Figure 7. The one-dimensional marginalization probability allocations for each parameter are shown in diagonal panels simultaneously, with their 68% confidence intervals. The two-dimensional relationship contours between couples of parameters are described in off diagonal panels; The plot denotes two confidence levels contours analogous to 1σ confidence level and 2σ confidence level, where the inner dark blue area shows the 1σ uncertainty and outer light

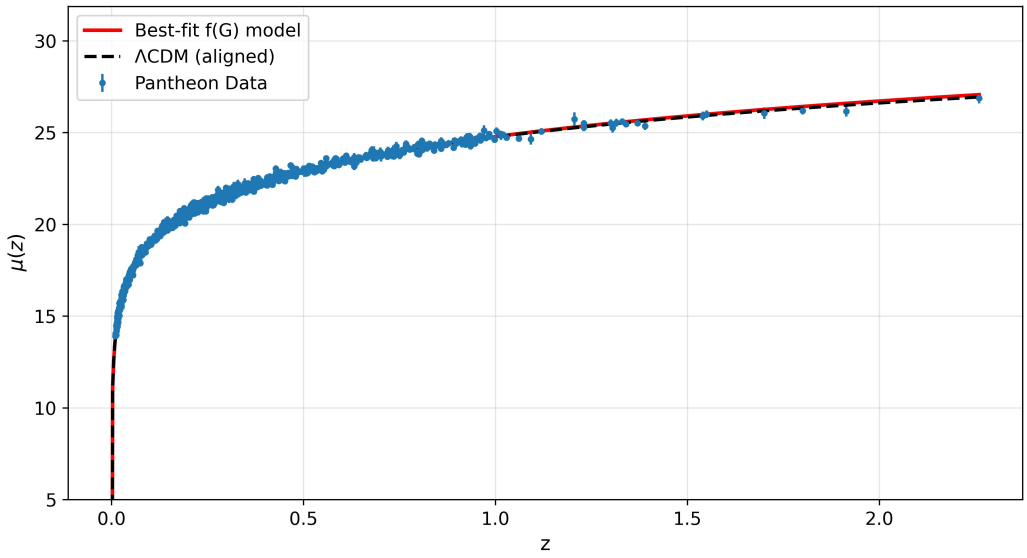

Figure 6: Comparison between the theoretical distance modulus $\mu(z)$ predicted by the reconstructed model (solid red line) and the Pantheon Supernova observations (blue data with error bars).

blue shaded region shows 2σ uncertainty. Due to Gaussian distributions, the parameters are highlight to be fine limitation, indicating true convergence and accurately evaluated. The model selection statistics show that $\mathrm{AIC}_{\mathrm{model}} = 75.9400$ and $\mathrm{BIC}_{\mathrm{model}} = 86.0704$ and $\mathrm{DIC}_{\mathrm{model}} = 71.9335$ with $\Delta\mathrm{AIC}_{\mathrm{model}} = -3.225$ and $\Delta\mathrm{BIC}_{\mathrm{model}} = -0.692$ and $\Delta\mathrm{DIC}_{\mathrm{model}} = -1.231$. An awesome consent among the model and the observational data is implicit by the reduced chi-square $\chi^2_{\mathrm{red}} = 0.7634$, which has the associated chi-square value at the MAP point, $\chi^2 = 67.9400$.

The combined allocations of the model parameter Ω_{m0}, H_0, σ_8, γ and M_B developed using a MCMC inspection using (RSD+Pantheon) dataset, are shown by the corner plot in Figure 8. The one-dimensional marginalization probability allocations for each parameter are shown in diagonal panels simultaneously, with their 68% confidence intervals. The two-dimensional relationship contours between couples of parameters are described in off diagonal panels; The plot denotes two confidence levels contours analogous to 1σ confidence level and 2σ confidence level, where the inner dark blue area shows the 1σ uncertainty and outer light blue shaded region shows 2σ uncertainty. Due to Gaussian distributions, the parameters are highlight to be fine limitation, indicating true convergence and accurately evaluated. The model selection statistics shows that $\mathrm{AIC}_{\mathrm{model}} = 791.1113$ and $\mathrm{BIC}_{\mathrm{model}} = 816.1718$ and $\mathrm{DIC}_{\mathrm{model}} = 786.8364$ with $\Delta\mathrm{AIC}_{\mathrm{model}} = -5.305$ and $\Delta\mathrm{BIC}_{\mathrm{model}} = -0.293$ and $\Delta\mathrm{DIC}_{\mathrm{model}} = -1.580$. An awesome consent among the model and the observational data is implicit by the reduced chi-square $\chi^2_{\mathrm{red}} = 0.7069$, which has the associated chi-square value at the MAP point, $\chi^2 = 781.1113$.

The combined allocations of the model parameter Ω_{m0}, H_0, γ and M_B developed using a MCMC inspection using (Hubble+Pantheon) dataset are shown by the corner plot in Figure 9. The one-dimensional marginalization probability allocations for each parameter are shown in diagonal panels simultaneously, with their 68% confidence intervals. The two-dimensional relationship contours between couples of parameters are described in off

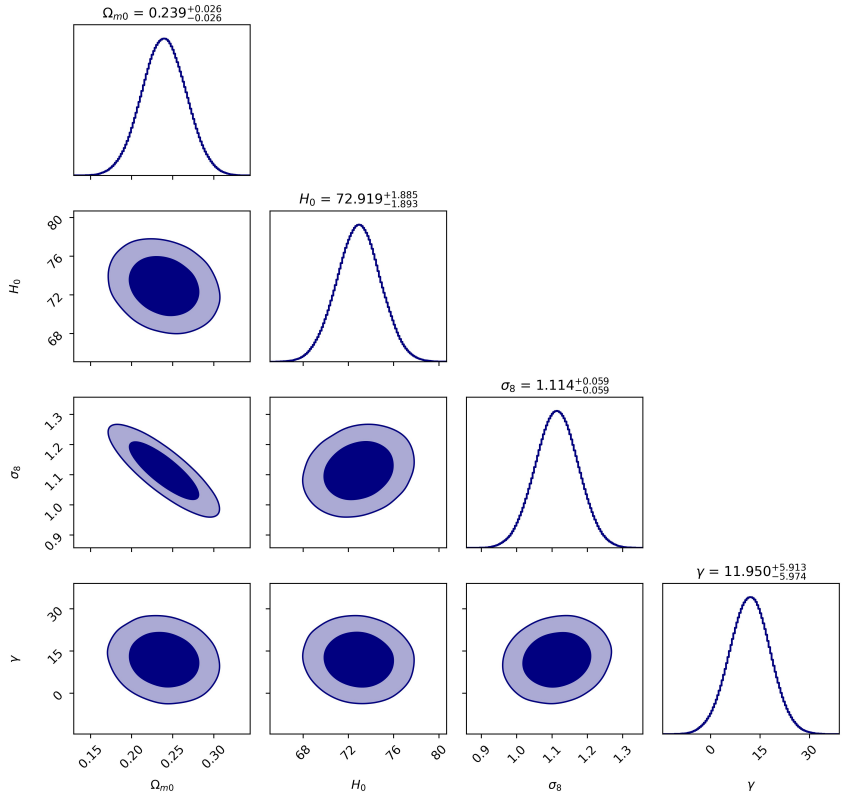

Figure 7: Confidence contours and marginalized posterior distributions for the parameters Ω_{m0}, H_0, $\sigma_8$and γ obtained from the (Hubble+RSD) dataset.

diagonal panels; The plot denotes two confidence levels contours analogous to 1σ confidence level and 2σ confidence level, where the inner dark blue area shows the 1σ uncertainty and outer light blue shaded region shows 2σ uncertainty. Due to Gaussian distributions, the parameters are highlight to be fine limitation, indicating true convergence and accurately evaluated. The model selection statistics shows that $\mathrm{AIC}_{\mathrm{model}} = 744.4765$ and $\mathrm{BIC}_{\mathrm{model}} = 764.4042$ and $\mathrm{DIC}_{\mathrm{model}} = 742.1116$ with $\Delta\mathrm{AIC}_{\mathrm{model}} = 5.878$ and $\Delta\mathrm{BIC}_{\mathrm{model}} = 10.860$ and $\Delta\mathrm{DIC}_{\mathrm{model}} = 9.514$. An awesome consent among the model and the observational data is implicit by the reduced chi-square $\chi^2_{\mathrm{red}} = 0.6864$, which has the associated chi-square value at the MAP point, $\chi^2 = 736.4765$.

Figure 10 gives corner plot demonstrating the joint posterior allocations and marginalized one-dimensional probability densities for the model having parameters Ω_{m0}, H_0 and γ obtained from the Hubble only, RSD only and (Hubble+RSD) combined datasets. The best-fit values over with their analogous 1σ confidence level and 2σ confidence level uncertainties are obtained as $\Omega_{m0} = 0.301^{+0.025}_{-0.020}$, $H_0 = 70.000^{+0.19}_{-0.18}$ and $\gamma = 0.9999^{+0.019}_{-0.018}$. The internal, darker contours show the 1σ confidence area, while the outer, lighter contours correspond to the 2σ confidence credible areas, indicating the extended spread of the parameter space. It can be followed that the combined (Hubble + RSD) dataset submits more rigorous and well-disciplined contours connected to the individual datasets, expertly reducing the parameter degradations and improving the general precision of the model constraints. This denotes the collaborative nature of Hubble and RSD observations in compelling cosmological parameters

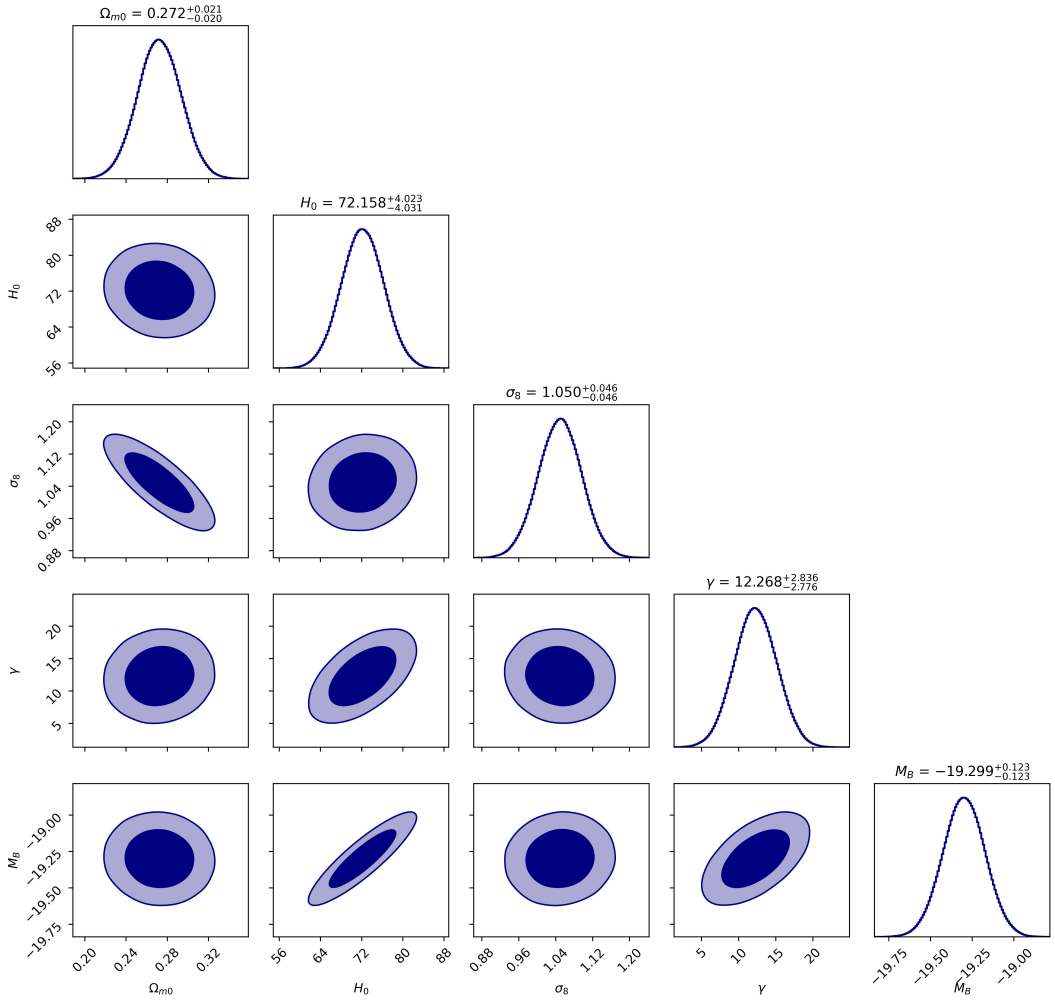

Figure 8: Confidence contours and marginalized posterior distributions for the parameters Ω_{m0}, H_0, σ_8, γ and M_B obtained from the (RSD+Pantheon) dataset.

within the adopted theoretical framework.

Figure 11 indicates the two dimensional RSD only Λ CDM constraints in the plane of (Ω_{0m}, σ_8). The blue shaded area indicates the 68%, 95%, 99.7%, and 99.994% confidence levels attained by fitting the $f\sigma_8(z)$ measurements which yields a best fit value of $\Omega_{0m} = 0.3222$ and $\sigma_8 = 0.6646$, shown by the green mark. The Pantheon Type Ia supernova data and Hubble data are displayed only for analogy in Ω_{0m}, with their associated data point placed at RSD best fit value of σ_8. The Pantheon Type Ia supernova prefer comparatively high matter density, $\Omega_{0m} \simeq 0.50$, indicated by red mark, which lies outside the confidence region of RSD, showing major tension between background expansion of Supernovae and growth rate dimensions inside ΛCDM for fixed H_0. In diverse, the Hubble data privilege $\Omega_{0m} \simeq 0.29$, indicated by orange mark, which is in significant consensus with RSD constraints. Overall, plot shows that RSD and Hubble data are jointly compatible, but the Pantheon dataset displays distinguished tension in associated with growth based

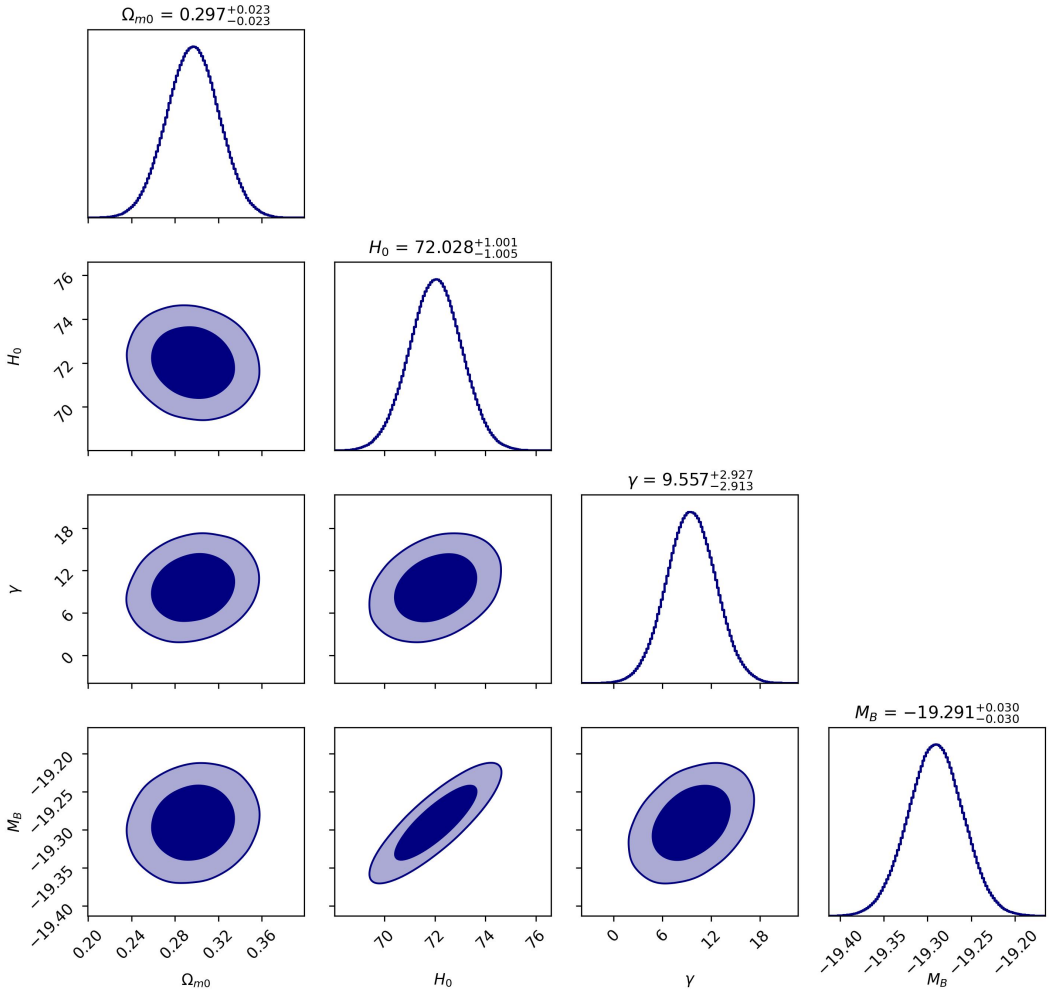

Figure 9: Confidence contours and marginalized posterior distributions for the parameters Ω_{m0}, H_0, γ and M_B obtained from the (Hubble+Pantheon) dataset.

constraints in the standard ΛCDM model equation (2.16).

After constraining model parameters, we need to verify energy conditions and stability analysis for completeness of the work in the next sections.

4 Energy conditions of the model

By using Equations (2.5),(2.6),(2.7),(2.8) and (2.9), we get the effective density and pressure as follows

$$\rho_{eff} = \rho + \frac{1}{\kappa^2}\Big[24H^2(H^2+\dot{H})f_G - f(G) - 576H^4(4H^2\dot{H} + 2\dot{H}^2 + H\ddot{H})f_{GG}\Big], \qquad (4.1)$$

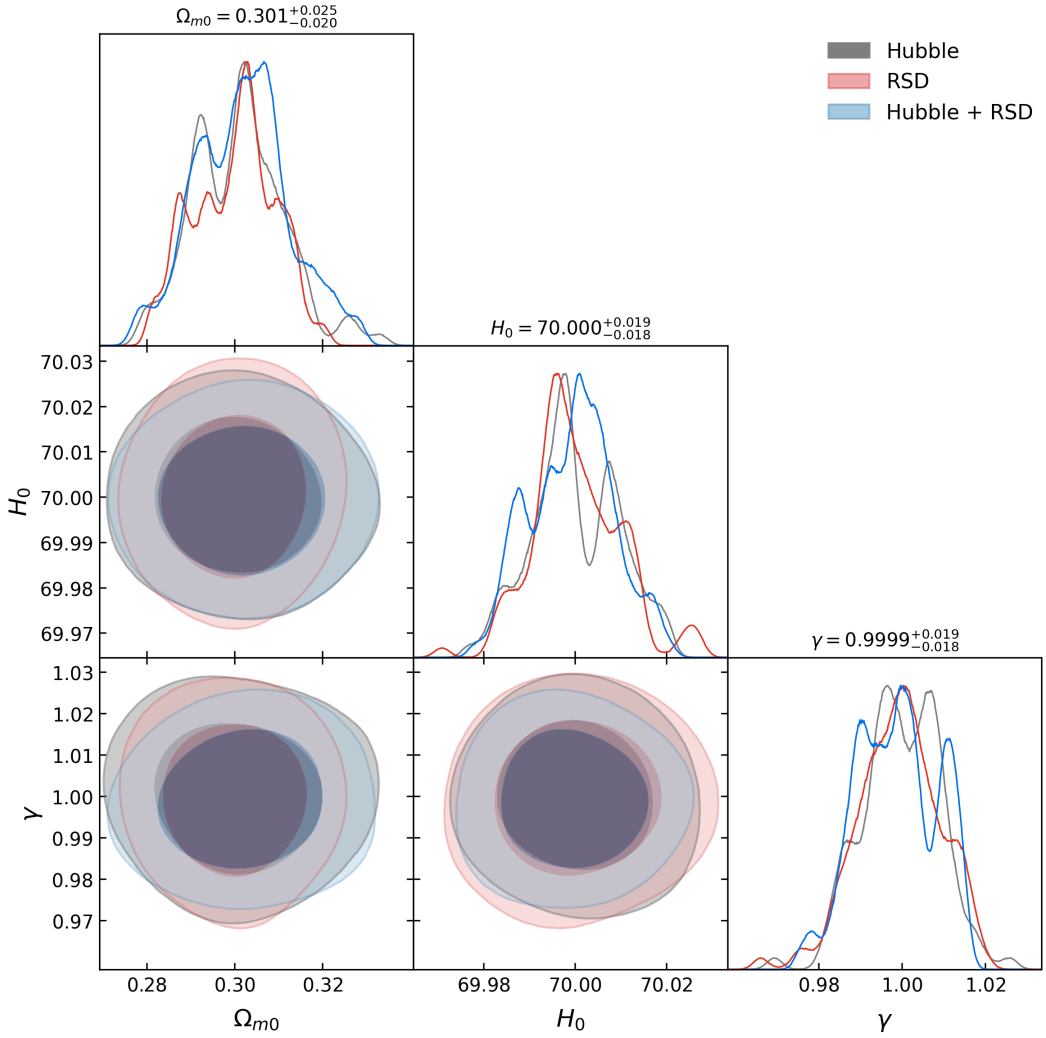

Figure 10: Confidence Mix overlay contours and marginalized posterior distributions for the parameters Ω_{m0}, H_0 and γ obtained from the Hubble only, RSD only and (Hubble+RSD) combined datasets.

$$p_{eff} = p + \frac{1}{\kappa^2}\Big[f(G) - 24H^2(H^2+\dot{H})f_G + 192H^2(12H^2\dot{H}^2 + 4H^3\ddot{H} + 2\dot{H}^3 + 6H\dot{H}\ddot{H} + H^2\dddot{H})f_{GG} + (24)^2 8H^4(2\dot{H}^2 + H\ddot{H} + 4H^2\dot{H})^2 f_{GGG}\Big]. \tag{4.2}$$

We also show the following expression

$$\rho_{eff} + p_{eff} = \rho + p + \frac{192H^2}{\kappa^2}\Big[(2\dot{H}^3 + 6H\dot{H}\ddot{H} + 6H^2\dot{H}^2 + H^3\ddot{H} - 12H^4\dot{H} + H^2\dddot{H})f_{GG} + 24H^2(2\dot{H}^2 + H\ddot{H} + 4H^2\dot{H})^2 f_{GGG}\Big] \tag{4.3}$$

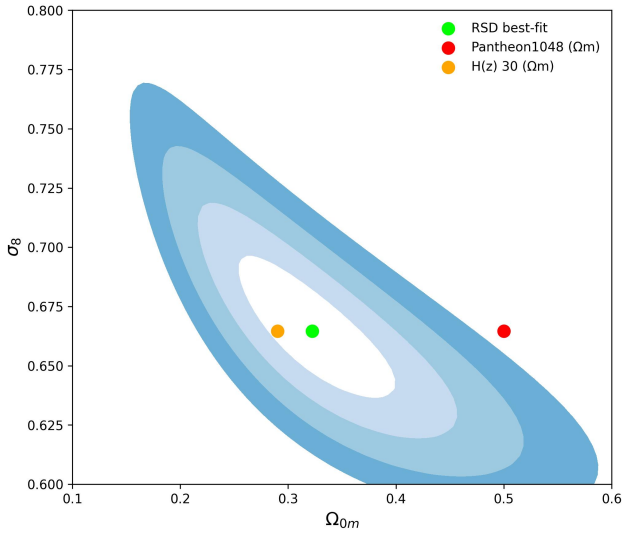

Figure 11: Joint confidene contours obtained from RSD in the (Ω_{0m}, σ_8) plane.

Table 1: Best-fit values of parameters for used model

Data used	**Parameters**	**Best fit values**
Hubble	Ω_{m0}	$0.3392^{+0.0707}_{-0.0568}$
	H_0	$69.5825^{+2.3170}_{-2.2941}$
	γ	$12.5591^{+5.1789}_{-4.0823}$
RSD	Ω_{m0}	$0.2129^{+0.0227}_{-0.0185}$
	H_0	$61.7727^{+8.9409}_{-8.3748}$
	γ	$13.6933^{+5.6105}_{-6.5713}$
	σ_8	$0.8064^{+0.0444}_{-0.0568}$
Pantheon	Ω_{m0}	$0.2977^{+0.0204}_{-0.0219}$
	H_0	$65.5346^{+3.2358}_{-2.6006}$
	γ	$5.9571^{+5.3240}_{-4.5481}$
Hubble+RSD	Ω_m	$0.239^{+0.026}_{-0.026}$
	H_0	$72.919^{+1.885}_{-1.893}$
	σ_8	$1.114^{+0.059}_{-0.059}$
	γ	$11.950^{+5.913}_{-5.974}$
RSD+Pantheon	Ω_m	$0.272^{+0.021}_{-0.020}$
	H_0	$72.158^{+4.023}_{-4.031}$
	σ_8	$1.050^{+0.046}_{-0.046}$
	γ	$12.268^{+2.836}_{-2.776}$
	M_B	$-19.299^{+0.123}_{-0.123}$
Hubble+Pantheon	Ω_m	$0.297^{+0.023}_{-0.023}$
	H_0	$72.028^{+1.001}_{-1.005}$
	γ	$9.557^{+2.927}_{-2.913}$
	M_B	$-19.291^{+0.030}_{-0.030}$

The energy conditions in the view of modified gravity, are given as [68]

Table 2: Statistical results for different datasets.

Data used	χ^2	**Reduced** χ^2	**AIC**	**BIC**	**DIC**	**ΔAIC**	**ΔBIC**	**ΔDIC**
Hubble	12.5165	0.4636	18.5165	22.7201	14.7835	2.4740	3.8752	2.7410
RSD	46.7288	0.7920	54.7288	63.3014	48.9108	5.3474	9.6337	3.5294
Pantheon	860.9189	0.8246	866.9189	881.7800	862.5687	4.8475	9.8011	4.4972
Hubble+RSD	67.9400	0.7634	75.9400	86.0704	71.9335	-3.225	-0.692	-1.231
RSD+Pantheon	781.1113	0.7069	791.1113	816.1718	786.8364	-5.305	-0.293	-1.580
Hubble+Pantheon	736.4765	0.6864	744.4765	764.4042	742.1116	5.878	10.860	9.514

i) Null Energy Condition (NEC)

$$\rho_{eff} + p_{eff} \geq 0. \tag{4.4}$$

ii) Weak Energy Condition (WEC)

$$\rho_{eff} \geq 0 \quad \text{and} \quad \rho_{eff} + p_{eff} \geq 0. \tag{4.5}$$

iii) Strong Energy Condition (SEC)

$$\rho_{eff} + 3p_{eff} \geq 0 \quad \text{and} \quad \rho_{eff} + p_{eff} \geq 0. \tag{4.6}$$

Now, in usual process, initial four time derivatives of position are stated as velocity, acceleration, jerk and snap. In a cosmological framework, additionally with the Hubble factor $H = \frac{\dot{a}}{a}$, the deceleration, jerk and snap variables is defined as [68]

$$q = -\frac{1}{H^2}\frac{\ddot{a}}{a}, \quad j = \frac{1}{H^3}\frac{\dddot{a}}{a}, \quad and \quad s = \frac{1}{H^4}\frac{\ddddot{a}}{a} \tag{4.7}$$

respectively.

Use the relations as given by [68]

$$\dot{H} = -H^2(1+q) \tag{4.8}$$

$$\ddot{H} = H^3(j+3q+2) \tag{4.9}$$

$$\dddot{H} = H^4(s-2j-5q-3) \tag{4.10}$$

By using Equations (4.8),(4.9), (4.10) in the Equations (4.1) and (4.3) then we get the following expressions

$$\rho_{eff} = \rho + \frac{1}{\kappa^2}\Big[-24H^4 q f_G - f(G) - 576H^8(2q^2+3q+j)f_{GG}\Big], \tag{4.11}$$

$$\begin{aligned}\rho_{eff} + p_{eff} =& \rho + p + \frac{192H^8}{\kappa^2}\Big[(-2q^3-18q^2-14q-6qj-7j+s+3)f_{GG} \\ &+ 24H^4(2q^2+3q+j)^2 f_{GGG}\Big].\end{aligned} \tag{4.12}$$

For these 3D plots, we have used numerical values for deceleration parameter ($q = -0.64$), for jerk parameter ($j = 1.02$) and for snap parameter ($s = -0.39$)[69]. Figure 12 shows that whole geometric surface is located above the zero for ρ_{eff}. No area of geometric surface drops into the negative values. So from the Figure 12, $\rho_{eff} > 0$ for $(0 < \gamma < 5)$ and $(0.5 < H < 1)$. So, the initial condition of WEC satisfied. Now, Figure 13 indicates that $(\rho_{eff} + p_{eff})$ stays positive for $0 < \gamma \lesssim 3.5$ and gives negative values for $\gamma > 3.5$. Hence

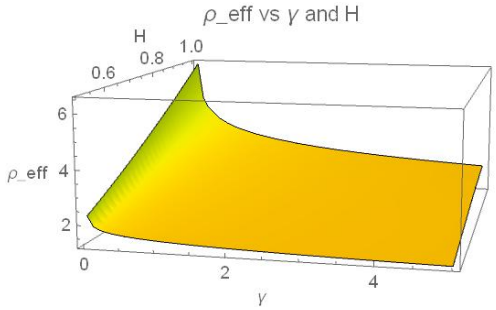

Figure 12: 3D-Evolution of effective energy density as a function of parameter γ and H

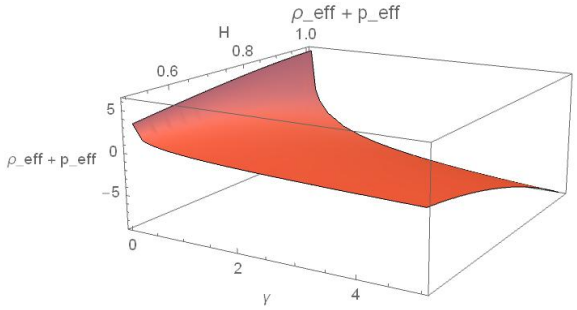

Figure 13: 3D-Evolution of combined effective energy density and pressure as a function of parameter γ and H

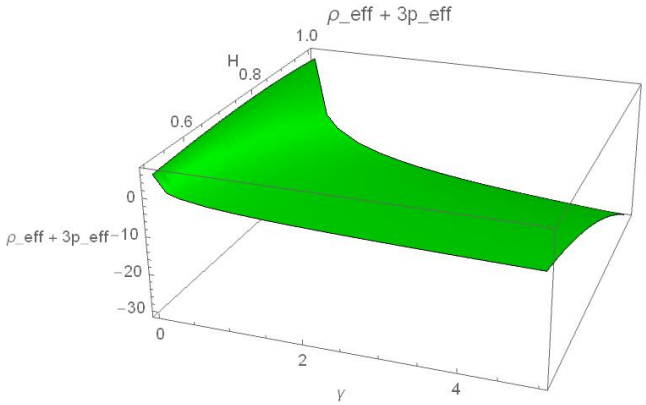

Figure 14: 3D-Evolution of $(\rho_{eff} + 3p_{eff})$ as a function of parameter γ and H

NEC satisfied for $0 < \gamma \lesssim 3.5$ and violated for $\gamma \gtrsim 3.5$. As, WEC needs both $\rho_{eff} \geq 0$ and $\rho_{eff} + p_{eff} \geq 0$. So, WEC depends overall on the comdition $\rho_{eff} + p_{eff} \geq 0$. Hence, the WEC gets satisfied for $0 < \gamma \lesssim 3.5$ and violated for $\gamma \gtrsim 3.5$. From the Figure 14, it is clear that quantity $(\rho_{eff} + 3p_{eff})$ becomes negative just after $\gamma \approx 1.2$. So the SEC gets violated for $\gamma \gtrsim 1.2$.

5 Stability assessment through dynamical system

For a general $f(G)$ model, consider the following variables [48]

$$x_1 = H^2 f_G, \quad x_2 = H\dot{f_G}, \quad x_3 = \frac{\dot{H}}{H^2}, \\ x_4 = \frac{-f}{6H^2}, \quad x_5 = \frac{\kappa^2\rho_r}{3H^2}, \tag{5.1}$$

Density parameters are

$$\Omega_m = \frac{\kappa^2\rho_m}{3H^2}, \quad \Omega_r = x_5 = \frac{\kappa^2\rho_r}{3H^2}, \quad \Omega_{DE} = \frac{\kappa^2\rho_{DE}}{3H^2}, \tag{5.2}$$

$$\Omega_m + \Omega_r + \Omega_{DE} = 1. \tag{5.3}$$

As, $N = ln(a)$

$$\frac{dx_1}{dN} = 2x_1x_3 + x_2 \tag{5.4}$$

$$\frac{dx_2}{dN} = x_2x_3 + (3x_1 - 2x_2)(1 + x_3) + \frac{(6x_4 - 2x_3 - x_5 - 3)}{8}, \tag{5.5}$$

$$\frac{dx_3}{dN} = \lambda - 2x_3^2, \tag{5.6}$$

$$\frac{dx_4}{dN} = -4x_1(4x_3 + 2x_3^2 + \lambda) - 2x_4x_3, \tag{5.7}$$

$$\frac{dx_5}{dN} = -2x_5(2 + x_3). \tag{5.8}$$

Logarithmic $f(G)$ model is

$$f(G) = \frac{\sqrt{3G}}{2} ln(\gamma G).$$

Consider $x_6 = ln(\gamma G)$

$$f(G) = \frac{\sqrt{3G}}{2} x_6, \\ \frac{dx_6}{dN} = \frac{1}{G}\frac{dG}{dN}. \tag{5.9}$$

As, $G = 24H^4(1 + x_3)$

$$\frac{dG}{dN} = 24H^4\Big[4x_3(1 + x_3) + \frac{dx_3}{dN}\Big], \tag{5.10}$$

$$\frac{dG}{dN} = G\Big[4x_3 + \frac{1}{1 + x_3}\frac{dx_3}{dN}\Big], \tag{5.11}$$

$$\frac{dx_6}{dN} = 4x_3 + \frac{\lambda - 2x_3^2}{1 + x_3}, \tag{5.12}$$

$$x_4 = -4x_1(1 + x_3)\frac{x_6}{\frac{x_6}{2} + 1}, \tag{5.13}$$

$$x_4 = -4x_1(1+x_3)\phi(x_6), \tag{5.14}$$

$$\frac{d\phi}{dx_6} = \phi'(x_6) = \frac{4}{(x_6+2)^2}, \tag{5.15}$$

from Equation (5.14)

$$\frac{dx_4}{dN} = -4\Big[(1+x_3)(2x_1x_3+x_2)\phi + x_1(\lambda-2x_3^2)\phi + 4x_1x_3(1+x_3)\phi' + x_1(\lambda-2x_3^2)\phi'\Big]. \tag{5.16}$$

To get the expression for $\lambda = \frac{\ddot{H}}{H^3}$, we have to equate Equations (5.7) and (5.16), then we get

$$\lambda = \frac{(1+x_3)(2x_1x_3+x_2)\phi + 2x_1x_3(1+x_3)\phi + 4x_1x_3(1+x_3)\phi' - x_1(4x_3+2x_3^2) - 2x_1x_3^2(\phi+\phi')}{x_1(1-\phi-\phi')} \tag{5.17}$$

Derivatives of dynamical system variables for critical points are as follows

$$\frac{dx_1}{dN} = 2x_1x_3 + x_2, \tag{5.18}$$

$$\frac{dx_2}{dN} = 3x_1x_3 + 3x_1 - x_2x_3 - 2x_2 - 3x_1(1+x_3)\phi - \frac{x_3}{4} - \frac{x_5}{8} - \frac{3}{8}, \tag{5.19}$$

$$\frac{dx_3}{dN} = \lambda - 2x_3^2, \tag{5.20}$$

$$\frac{dx_5}{dN} = -2x_5(2+x_3). \tag{5.21}$$

For critical point examination

$$\frac{dx_1}{dN} = 0, \quad \frac{dx_2}{dN} = 0, \quad \frac{dx_3}{dN} = 0, \quad \frac{dx_5}{dN} = 0. \tag{5.22}$$

Eigen values gets

$$\lambda_1 = -4x_1,$$

and

$$\lambda_2 = -2(2+x_3).$$

5.1 Stability associated with critical points using Eigen value

Critical points are
Point: 1

$$x_1 = \frac{\frac{x_3}{4} + \frac{3}{8}}{2x_3^2 + 7x_3 + 3 - 3(1+x_3)\phi}, \quad x_2 = -2x_1x_3, \quad x_3 = \sqrt{\frac{\lambda}{2}}, \quad x_5 = 0. \tag{5.23}$$

Point: 2

$$x_1 = \frac{\frac{x_3}{4} + \frac{3}{8}}{2x_3^2 + 7x_3 + 3 - 3(1+x_3)\phi}, \quad x_2 = -2x_1x_3, \quad x_3 = -\sqrt{\frac{\lambda}{2}}, \quad x_5 = 0. \tag{5.24}$$

Point: 3

$$x_1 = \frac{-1}{24(\phi-1)}, \quad x_2 = 4x_1, \quad x_3 = -2, \quad x_5 = 0. \tag{5.25}$$

Point: 4

$$x_1 = \frac{x_5 - 1}{24(\phi-1)}, \quad x_2 = 4x_1, \quad x_3 = -2, \quad x_5 = 0. \tag{5.26}$$

Table 3: Stability domain of critical points

Critical point	**Stability**	**Remark**
$\mathcal{P}_1$	Stable	satisfies the eigen values
$\mathcal{P}_2$	Unstable	for negative $x_3 = -\sqrt{\frac{\lambda}{2}}$,$-4x_3 > 0$
$\mathcal{P}_3$	Unstable	for $\lambda_1 = 8 > 0$, $\lambda_2 = 0$
$\mathcal{P}_4$	Unstable	for $\lambda_1 = 8 > 0$, $\lambda_2 = 0$

5.2 Stability associated with critical points using phase space diagram

Figure 15 shows the two-dimensional phase space plot for the dynamical system variables x_1 and x_2. Plots (a), (b), (c), and (d) are associated with the critical points $\mathcal{P}_1$, $\mathcal{P}_2$, $\mathcal{P}_3$, and $\mathcal{P}_4$ respectively. Stability nature of the critical points can be analysed on the basis of phase space curves given in the Figure 15. For the point $\mathcal{P}_1$, curves approach the point over particular directions but deviates along others. So, point $\mathcal{P}_1$ attains saddle type character, which indicating the instability on the basis of phase space. As, point $\mathcal{P}_2$ indicates stable point (curves attractor) nature, as all locally around curves converges monotonically towards the point from vibrant directions which confirming asymptotic stability. Point $\mathcal{P}_3$ acts like a attracting spiral point where curves rotate while moving toward the point, highlighting decaying oscillatory stability. Point $\mathcal{P}_4$ also illustrates a saddle point nature, with phase curves deviating away over one region and converging over another region which leading to unstable nature. Overall, points $\mathcal{P}_2$ and $\mathcal{P}_3$ are stable, while points $\mathcal{P}_1$ and $\mathcal{P}_4$ are unstable saddle points.

6 Conclusion

The cosmological action of a complex modified Gauss-Bonnet (GB) gravity model gets examined in this work. As a fundamental terms in cosmological era i.e Ricci scalar and Gauss Bonnet invariant, were initially covered. Next, we attained the point-like Lagrangian theories and associated equations of motions under the view of flat FLRW cosmic background. In this work, we focused on a specific logarithmic function given by $f(G) = \frac{\sqrt{3}}{2}\sqrt{G}\, ln(\gamma G)$, which directs General Relativity theory and where real constant α gets tends to zero. Our analysis is especially fascinating as a possible substitute for the conventional Λ CDM model because it does not explicitly assemble to the cosmological constant condition. This model prevents the conceptual problems associated to Λ while demonstrating the ability to propagate dark energy (DE) actions. We have demonstrated that the right-hand side of modified Friedmann equations can be interpreted as effective energy density and pressure generated about by curvature. We looked for cosmological attributes of $f(G)$ model when matter fields

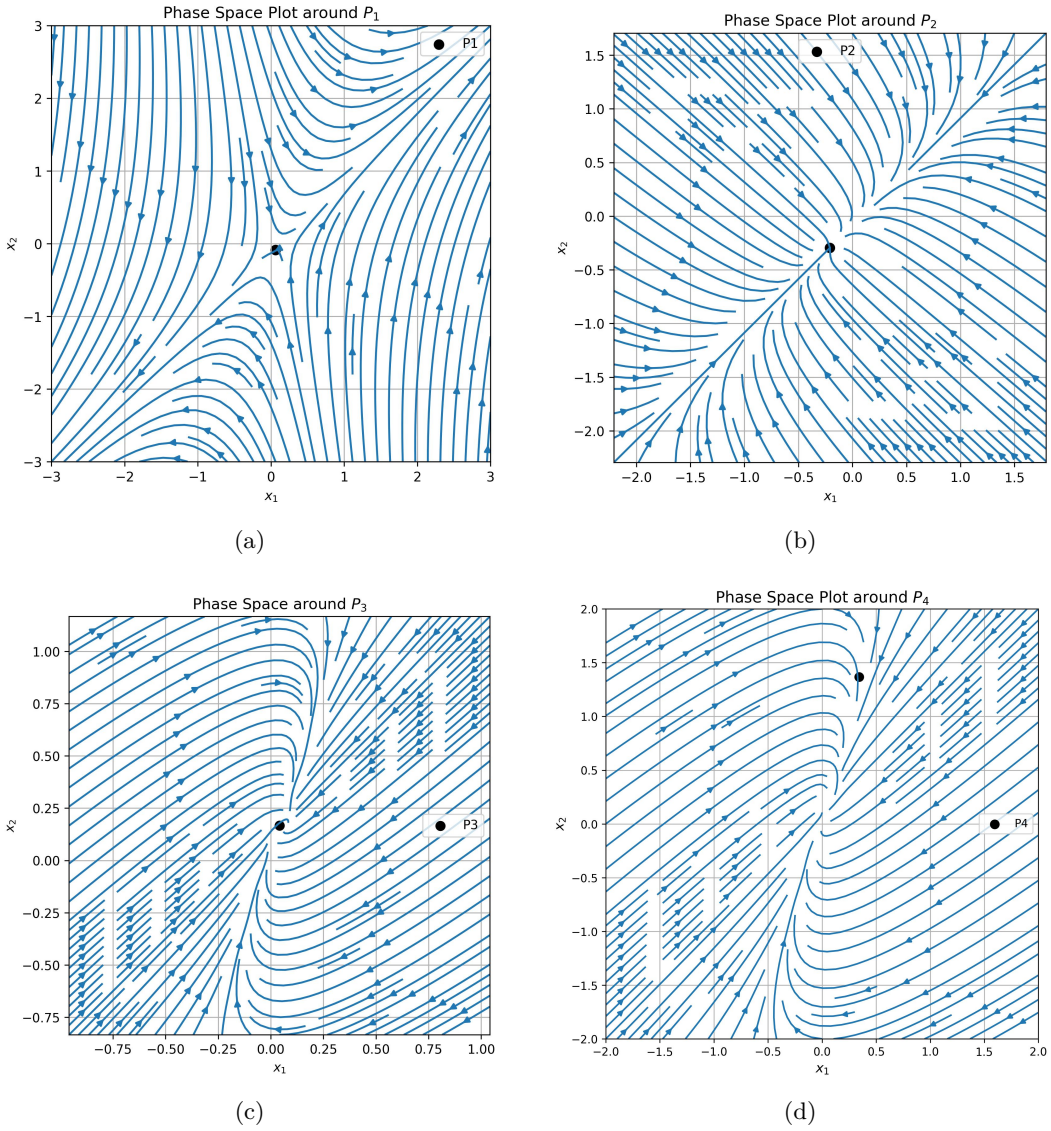

Figure 15: 2D-Phase space plot for the dynamical system variable x_1 and x_2

were encompassed. We despised the radiation fluid's late-time contribution and assumed non-relativistic pressure-less matter. We were able to learn the Hubble parameter's redshift behavior by numerically solving the modified Friedmann equation. We have worked for the ΛCDM model to determine the suitable inception conditions for Hubble parameter as a function of redshift z i.e $H(z)$ and its derivatives. In particular, we have used Bayesian statistical method which is based on Markov Chain Monte Carlo (MCMC) approach. In association with MCMC, we have used Hubble dataset, RSD and Pantheon+ dataset. We attained restrictions on the model's free parameters at the 1σ and 2σ confidence levels by assuming uniform prior distributions. This permitted us to recreate the cosmic evolution of the total effective equation of state (EoS) parameter and the Hubble expansion rate. According to our research, the $f(G)$ model decently explained the current acceleration of the Universe in

absent with the necessity for a cosmological constant Λ. Our investigation reveals a major difference between the H_0 values derived from the Hubble dataset, Pantheon+ dataset and RSD analysis underscoring the persistent H_0 tension in cosmology. This finding highlights the need for additional investigation into potential systemic flaws or novel physics to address this problem.

From Figure 12, 13 and 14, we have illustrated the Energy conditions of model in Section 4. According to this examination, NEC satisfied for $0 < \gamma \lesssim 3.5$ and violated for $\gamma \gtrsim 3.5$. Also, the WEC gets satisfied for $0 < \gamma \lesssim 3.5$ and violated for $\gamma \gtrsim 3.5$.And the SEC gets violated for $\gamma \gtrsim 1.2$. In the Section 5, we have discussed the stability of model on the basis of dynamical system mechanism. In which, stability is attained for Critical point $\mathcal{P}_1$ and gets unstability for critical points $\mathcal{P}_2$, $\mathcal{P}_3$ and $\mathcal{P}_4$ as shown in Table 3. From the Figure 15, we have examined the stability through the phase space curves in association with critical points $\mathcal{P}_1$, $\mathcal{P}_2$, $\mathcal{P}_3$, and $\mathcal{P}_4$ in the section 5.2. From this, we have illustrated that the points $\mathcal{P}_2$ and $\mathcal{P}_3$ are stable, while points $\mathcal{P}_1$ and $\mathcal{P}_4$ are unstable saddle points. Improving our comprehension of the universe's expanding rate requires resolving these disparities. To beyond test the feasibility of the proposed model in the $f(G)$ gravity, we decide to extend our investigation by incorporating additional observational data, like Redshift Space Distortion (RSD) measurement, DESI data and the Union3 supernova compilation. We also aim to examine the perturbative rule of the proposed model to investigate the large-scale structures growth by using RSD data. In extension, we plan to interrogate the implications of $f(G)$ gravity for current cosmological tensions, besides the H_0 and S_8 distinctness, by incorporating Cosmic Microwave Background (CMB) data. These extensions will be pursued in future work.

Authors' Contributions

M. T. conceptualized the study and wrote the initial draft. P. K. D. carried out the analytical calculations. A. M. performed numerical simulations and data analysis. S. I. supervised the research and contributed to manuscript revision. All authors reviewed and approved the final version of the manuscript.

Data Availability

The manuscript has no associated data or the data will not be deposited.

Conflicts of Interest

The authors declare that there is no conflict of interest.

Ethical Considerations

The authors have diligently addressed ethical concerns, such as informed consent, plagiarism, data fabrication, misconduct, falsification, double publication, redundancy, submission, and other related matters.

Acknowledgment

MT gratefully acknowledges for JRF from DST-INSPIRE Fellowship (IF230556), Department of Science and Technology, Ministry of Science and Technology, government of India. PKD wish to mention that the part of the numerical computation of this work was carried out on the Pegasus Computing Cluster of IUCAA, Pune, India and also acknowledges the Inter-University Centre for Astronomy and Astrophysics (IUCAA), Pune, India, for providing him a Visiting Associateship under which a part of this work was carried out. AM acknowledges the hospitality of the University of Rwanda-College of Science and Technology, where part of this work was conceptualized and completed.

References

[1] Misner, C.W., Thorne, K.S. & Wheeler, J.A., "Gravitation", Macmillan **(1973)**. https://physicsgg.me/wp-content/uploads/2023/05/misner_thorne_wheeler_gravitation_freema.pdf

[2] Bertone, G., Hooper, D. & Silk, J., "Particle dark matter: Evidence, candidates and constraints", Phys. Rept., **405**(279), (2005). DOI: https://doi.org/10.1016/j.physrep.2004.08.031

[3] Copeland, E.J., Sami, M. & Tsujikawa, S., "Dynamics of dark energy", International Journal of Modern Physics D, **15**(1753), (2006). DOI: https://doi.org/10.1142/S021827180600942X

[4] Riess, A.G., Filippenko, A.V., Challis, P., Clocchiatti, A., Diercks, A., Garnavich, P.M., & et al., "Observational evidence from supernovae for an accelerating universe and a cosmological constant", The astronomical journal, **116**(1009), (1998). DOI: https://doi.org/10.1086/300499

[5] Will, C.M., "The confrontation between general relativity and experiment", Living reviews in relativity, **17**(1), (2014). DOI: https://doi.org/10.12942/lrr-2014-4

[6] Clifton, T., Ferreira, P.G., Padilla, A. & Skordis, C., "Modified gravity and cosmology", Physics reports, **513**(1), (2012). DOI: https://doi.org/10.1016/j.physrep.2012.01.001

[7] Adame, A.G., Aguilar, J., Ahlen, S., Alam, S., Alexander, D.M., Alvarez, M., & et al., "DESI 2024 VI: cosmological constraints from the measurements of baryon acoustic oscillations", Journal of Cosmology and Astroparticle Physics, **2**(021), (2025). DOI: https://doi.org/10.1088/1475-7516/2025/02/021

[8] Perlmutter, S., Aldering, G., Goldhaber, G., Knop, R.A., Nugent, P., Castro, P.G. & Supernova Cosmology Project, "Measurements of Ω and Λ from 42 high-redshift supernovae", The Astrophysical Journal, **517**(565), (1999). DOI: https://doi.org/10.1086/307221

[9] Spergel, D.N., Verde, L., Peiris, H.V., Komatsu, E., Nolta, M.R., Bennett, C.L., & et al., "First-year Wilkinson Microwave Anisotropy Probe (WMAP)* observations: determination of cosmological parameters", The Astrophysical Journal Supplement Series, **148**(175), (2003). DOI: https://doi.org/10.1086/377226

[10] Hinshaw, G., Larson, D., Komatsu, E., Spergel, D.N., Bennett, C., Dunkley, J., & et al., "Nine-year Wilkinson Microwave Anisotropy Probe (WMAP) observations: cosmological parameter results", The Astrophysical Journal Supplement Series, **208**(19), (2013). DOI: https://doi.org/10.1088/0067-0049/208/2/19

[11] Alam, S., Ata, M., Bailey, S., Beutler, F., Bizyaev, D., Blazek, J.A., & et al., "The clustering of galaxies in the completed SDSS-III Baryon Oscillation Spectroscopic Survey: cosmological analysis of the DR12 galaxy sample", Monthly Notices of the Royal Astronomical Society, **470**(2617), (2017). DOI: https://doi.org/10.1093/mnras/stx721

[12] Eisenstein, D.J., Zehavi, I., Hogg, D.W., Scoccimarro, R., Blanton, M.R., Nichol, R.C., & et al., "Detection of the baryon acoustic peak in the large-scale correlation function of SDSS luminous red galaxies", The Astrophysical Journal, **633**(560), (2005). DOI: https://doi.org/10.1086/466512

[13] Nojiri, S.I. & Odintsov, S.D., "Introduction to modified gravity and gravitational alternative for dark energy", International Journal of Geometric Methods in Modern Physics, **4**(115), (2007). DOI: https://doi.org/10.1142/S0219887807001928

[14] Cartier, C., Copeland, E.J. & Madden, R., "The graceful exit in string cosmology", Journal of High Energy Physics, **2000**(035), (2000). DOI: https://doi.org/10.48550/arXiv.hep-th/9711134

[15] Gasperini, M. & Veneziano, G., "The pre-big bang scenario in string cosmology", Physics Reports, **373**(1), (2003). DOI: https://doi.org/10.1016/S0370-1573%2802%2900389-7

[16] Capozziello, S. & Francaviglia, M., "Extended theories of gravity and their cosmological and astrophysical applications", General Relativity and Gravitation, **40**(357), (2008). DOI: https://doi.org/10.1007/s10714-007-0551-y

[17] Nojiri, S.I. & Odintsov, S.D., "Modified Gauss–Bonnet theory as gravitational alternative for dark energy", Physics Letters B, **631**(1), (2005). DOI: https://doi.org/10.1016/j.physletb.2005.10.010

[18] Li, B., Barrow, J.D. & Mota, D.F., "Cosmology of modified Gauss-Bonnet gravity", Physical Review D—Particles, Fields, Gravitation, and Cosmology, **76**(044027), (2007). DOI: https://doi.org/10.1103/PhysRevD.76.044027

[19] Nojiri, S.I., Odintsov, S.D. & Tretyakov, P.V., "From inflation to dark energy in the non-minimal modified gravity", Progress of Theoretical Physics Supplement, **172**(81), (2008). DOI: https://doi.org/10.1143/PTPS.172.81

[20] De Felice, A. & Tsujikawa, S., "Solar system constraints on f (G) gravity models", Physical Review D—Particles, Fields, Gravitation, and Cosmology, **80**(063516), (2009). DOI: https://doi.org/10.1103/PhysRevD.80.063516

[21] Elizalde, E., Myrzakulov, R., Obukhov, V.V. & Sáez-Gómez, D., "ΛCDM epoch reconstruction from F (R, G) and modified Gauss–Bonnet gravities", Classical and Quantum Gravity, **27**(095007), (2010). DOI: 10.1088/0264-9381/27/9/095007

[22] Nojiri, S.S.D.O., Odintsov, S.D. & Oikonomou, V., "Modified gravity theories on a nutshell: Inflation, bounce and late-time evolution", Physics Reports, **692**(1), (2017). DOI: https://doi.org/10.1016/j.physrep.2017.06.001

[23] Odintsov, S.D., Oikonomou, V.K. & Banerjee, S., "Dynamics of inflation and dark energy from F (R, G) gravity", Nuclear Physics B, **938**(935), (2019). DOI: https://doi.org/10.1016/j.nuclphysb.2018.07.013

[24] Maurya, S.K., Pradhan, A., Tello-Ortiz, F., Banerjee, A. & Nag, R., "Minimally deformed anisotropic stars by gravitational decoupling in Einstein–Gauss–Bonnet gravity", The European Physical Journal C, **81**(848), (2021). DOI: https://doi.org/10.1140/epjc/s10052-021-09628-1

[25] Maurya, S.K., Singh, K.N., Govender, M. & Hansraj, S., "Gravitationally decoupled strange star model beyond the standard maximum mass limit in Einstein–Gauss–Bonnet gravity", The Astrophysical Journal, **925**(208), (2022). DOI: 10.3847/1538-4357/ac4255

[26] Lohakare, S.V., Rathore, K. & Mishra, B., "Observational constrained $F(R,\mathcal{G})$ gravity cosmological model and the dynamical system analysis", Classical and Quantum Gravity, **40**(215009), (2023). DOI: 10.1088/1361-6382/acfc0f

[27] Stelle, K.S., "Classical gravity with higher derivatives", General Relativity and Gravitation, **9**(353), (1978). DOI: https://doi.org/10.1007/BF00760427

[28] Nojiri, S.I., Odintsov, S.D. & Gorbunova, O.G., "Dark energy problem: from phantom theory to modified Gauss–Bonnet gravity", Journal of Physics A: Mathematical and General, **39**(6627), (2006). DOI: 10.1088/0305-4470/39/21/S62

[29] Barth, N.H. & Christensen, S.M., "Quantizing fourth-order gravity theories: The functional integral", Physical Review D, **28**(1876), (1983). DOI: https://doi.org/10.1103/PhysRevD.28.1876

[30] De Felice, A. & Suyama, T., "Scalar mode propagation in modified gravity with a scalar field", Physical Review D—Particles, Fields,Gravitation, and Cosmology, **80**(083523), (2009). DOI: https://doi.org/10.1103/PhysRevD.80.083523

[31] Peebles, P.J.E. & Ratra, B., "The cosmological constant and dark energy", Reviews of modern physics, **75**(559), (2003). DOI: https://doi.org/10.1103/RevModPhys.75.559

[32] Nojiri, S.I. & Odintsov, S.D., "Unified cosmic history in modified gravity: from F (R) theory to Lorentz non-invariant models", Physics Reports, **505**(59), (2011). DOI: https://doi.org/10.1016/j.physrep.2011.04.001

[33] Joyce, A., Lombriser, L. & Schmidt, F., "Dark energy versus modified gravity", Annual Review of Nuclear and Particle Science, **66**(95), (2016). DOI: https://doi.org/10.1146/annurev-nucl-102115-044553

[34] Cognola, G., Elizalde, E., Nojiri, S.I., Odintsov, S.D. & Zerbini, S., "Dark energy in modified Gauss-Bonnet gravity: Late-time acceleration and<? format?> the hierarchy problem", Physical Review D—Particles, Fields, Gravitation, and Cosmology, **73**(084007), (2006). DOI: https://doi.org/10.1103/PhysRevD.73.084007

[35] Rajantie, A., Contaldi, C., Dauncey, P. & Stoica, H., "PARTICLES, STRINGS, AND COSMOLOGY" 13th International Symposium on Particles, Strings, and Cosmology-PASCOS 2007, Particles, Strings, and Cosmology-PASCOS, (2007). DOI: https://ui.adsabs.harvard.edu/abs/2007AIPC..957.....R

[36] Anagnostopoulos, F.K., Basilakos, S. & Saridakis, E.N., "Bayesian analysis of $f(T)$ gravity using $f\sigma_8$ data", Physical Review D, **100**(083517), (2019). DOI: https://doi.org/10.1103/PhysRevD.100.083517

[37] Iorio, L. & Saridakis, E.N., "Solar system constraints on f (T) gravity", Monthly Notices of the Royal Astronomical Society, **427**(1555), (2012). DOI: https://doi.org/10.1111/j.1365-2966.2012.21995.x

[38] Capozziello, S., Luongo, O. & Saridakis, E.N., "Transition redshift in f (T) cosmology and observational constraints", Physical Review D, **91**(124037), (2015). DOI: https://doi.org/10.1103/PhysRevD.91.124037

[39] Bonici, M. & Maggiore, N., "Constraints on interacting dynamical dark energy and a new test for Λ CDM", The European Physical Journal C, **97**(672), (2019). DOI: https://doi.org/10.1140/epjc/s10052-019-7198-1

[40] Pan, S. & Yang, W., "On the Interacting Dark Energy Scenarios—The Case for Hubble Constant Tension", The European Physical Journal C, (2024). DOI: https://doi.org/10.1007/978-981-99-0177-7_29

[41] Wang, D., "Constraining cosmological physics with DESI BAO observations", arXiv:2404.06796, (2024). DOI: https://doi.org/10.48550/arXiv.2404.06796

[42] Pang, Y.H., Zhang, X. & Huang, Q.G., "Reevaluating H_0 Tension with Non-Planck CMB and DESI BAO Joint Analysis", arXiv:2411.14189, (2024). DOI: https://doi.org/10.48550/arXiv.2411.14189

[43] Zheng, J., Qiang, D.C. & You, Z.Q., "Cosmological constraints on dark energy models using DESI BAO 2024", arXiv:2412.04830, (2024). DOI: https://doi.org/10.1088/1475-7516/2025/08/056

[44] Makarenko, A.N. & Myagky, A.N., "The asymptotic behavior of bouncing cosmological models in F (G) gravity theory", International Journal of Geometric Methods in Modern Physics, **14**(1750148), (2017). DOI: https://doi.org/10.1142/S0219887817501481

[45] Munyeshyaka, A., Ntahompagaze, J., Mutabazi, T. & Mbonye, M., "On covariant perturbations with scalar field in modified Gauss–Bonnet gravity", The European Physical Journal C, **84**(51), (2024). DOI: https://doi.org/10.1140/epjc/s10052-023-12381-2

[46] Nojiri, S. & Odintsov, S.D., "Modified Gauss–Bonnet theory as gravitational alternative for dark energy", Physics Letters B, **631**(1), (2005). DOI: https://doi.org/10.1016/j.physletb.2005.10.010

[47] Lee, S. & Tumurtushaa, G., "The viable f (G) gravity models via reconstruction from the observations", Journal of Cosmology and Astroparticle Physics, **2020**(029), (2020). DOI: https://doi.org/10.1088/1475-7516/2020/06/029

[48] Lohakare, S.V., Niyogi, S. & Mishra, B., "Cosmology in modified $f(G)$ gravity: a late-time cosmic phenomena", Monthly Notices of the Royal Astronomical Society, **535**(1136), (2024). DOI: https://doi.org/10.1093/mnras/stae2302

[49] Kilbinger, M., et al., "Bayesian model comparison in cosmology with Population Monte Carlo", Monthly Notices of the Royal Astronomical Society, **405**(2381), (2010). DOI: https://doi.org/10.1111/j.1365-2966.2010.16605.x

[50] Brout, D., et al., "The Pantheon plus analysis: cosmological constraints", The Astrophysical Journal, **938**(110), (2022). DOI: 10.3847/1538-4357/ac8e04

[51] Sharov, G.S. & Vorontsova, E.G., "Parameters of cosmological models and recent astronomical observations", Journal of Cosmology and Astroparticle Physics 2014, **10**(057), (2014). DOI: https://doi.org/10.1088/1475-7516/2014/10/057

[52] Akaike, H., "A new look at the statistical model identification", IEEE transactions on automatic control, **19**(716), (2003). DOI: https://doi.org/10.1109/TAC.1974.1100705

[53] Vrieze, S.I., "Model selection and psychological theory: a discussion of the differences between the Akaike information criterion (AIC) and the Bayesian information criterion (BIC)", Psychological methods, **17**(228), (2012). DOI: https://doi.org/10.1037/a0027127

[54] Errahmani, A. et al., "Emergence of running vacuum energy in f(R, T) gravity : Observational constraints", Physics Letters B, **872**(140040), (2026). DOI: https://doi.org/10.48550/arXiv.2502.18193

[55] Liddle, A.R., "Information criteria for astrophysical model selection", Monthly Notices of the Royal Astronomical Society: Letters, **377**(L74), (2007). DOI: https://doi.org/10.1111/j.1745-3933.2007.00306.x

[56] Singh, G.P. & Kale, A.Y., "Anisotropic bulk viscous cosmological models with particle creation", Astrophys Space Sci, **331**(207), (2011). DOI: https://doi.org/10.1007/s10509-010-0400-4

[57] Singh, G.P., Deshpande, R.V. & Singh, T., "Higher-dimensional cosmological model with variable gravitational constant and bulk viscosity in Lyra geometry", Pramana - J Phys, **63**(937), (2004). DOI: https://doi.org/10.1007/BF02704332

[58] Kazantzidis, L. & Perivolaropoulos, L., "Evolution of the f σ 8 tension with the Planck 15/Λ CDM determination and implications for modified gravity theories", Physical Review D, **97**(103503), (2018). DOI: https://doi.org/10.1103/PhysRevD.97.103503

[59] Dhankar, P.K., Sanyal, A., Munyeshyaka, A., Ray, S. & Pourhassan, B., "Observational analysis of bulk viscous modified Chaplygin gas in (2+1)-dimensional universe using MCMC", arXiv:2504.18612, (2025). DOI: https://doi.org/10.48550/arXiv.2504.18612

[60] Dhankar, P.K., Munyeshyaka, A., Sanyal, A., Islam, S. & Rahaman, F., "Constraints on multi-fluid cosmology in modified Gauss-Bonnet gravity models with different observational data sets", arXiv preprint arXiv:2507.22191, (2025). DOI: https://doi.org/10.48550/arXiv.2507.22191

[61] Thakre, M., Dhankar, P.K., Islam, S., Sahoo, P., Rahaman, F. & Pourhassan, B., "A Bayesian Statistical Study of Bianchi Type-I Universe in $f(R, T^{\psi})$ Modified Gravity", arXiv preprint arXiv:2601.03116, (2026). DOI: https://doi.org/10.48550/arXiv.2601.03116

[62] Thakre, M., Dhankar, P.K., Pourhassan, B. & Islam, S., "Viscous Fluid Models of Cosmic Acceleration in FRW Spacetime Using MCMC Constraints", arXiv preprint arXiv:2511.03258, (2025). DOI: https://doi.org/10.48550/arXiv.2511.03258

[63] Mune, M., Dhankar, P.K., Islam, S., Pourhassan, B., Aamir, M. & Haroon, F., "Statistical Constraints on Anisotropic Bianchi-III Cosmology in $f(R,T)$-Gravity Using MCMC Methods", arXiv preprint arXiv:2510.19852, (2025). DOI: https://doi.org/10.48550/arXiv.2510.19852

[64] Dhankar, P.K., Sanyal, A., Islam, S., Rahaman, F. & Pourhassan, B., "Testing the Generalized Second Law in (2 + 1)-Dimensional Cosmology: Holographic Entropy Bounds and Observational Constraints", arXiv preprint arXiv:2508.13227, (2025). DOI: https://doi.org/10.48550/arXiv.2508.13227

[65] Kumar, D., Dhankar, P.K., Ray, S. & Zhang, F., "Joint analysis of constraints on f (R) parametrization from recent cosmological observations", Physics of the Dark Universe, **49**(101989), (2025). DOI: https://doi.org/10.1016/j.dark.2025.101989

[66] Dhankar, P.K., Mhamdi, D., Munyeshyaka, A., Kumar, D., Ntahompagaze, J. & Ouali, T., "Testing gauss-bonnet gravity with desi bao data", arXiv preprint arXiv:2508.03602, (2025). DOI: https://doi.org/10.1140/epjc/s10052-026-15607-1

[67] Patel, R., Dhankar, P.K., Islam, S. & Aamir, M., "Data analysis in (2+ 1)-D $\Lambda(z)$ gravity with BAO, Pantheon and Hubble dataset using MCMC method", Indian Journal of Physics, (2026). DOI: https://doi.org/10.1007/s12648-026-03982-0

[68] Garcia, N.M., Harko, T., Lobo, F.S. & Mimoso, J.P., "Energy conditions in modified Gauss-Bonnet gravity", Physical Review D—Particles, Fields, Gravitation, and Cosmology, **83**(104032), (2011). DOI: https://doi.org/10.1103/PhysRevD.83.104032

[69] Bamba, K., Ilyas, M., Bhatti, M.Z. & Yousaf, Z., "Energy conditions in modified f (G) gravity", General Relativity and Gravitation, **49**(112), (2017). DOI: https://doi.org/10.1007/s10714-017-2276-x